We thank the reviewers for their helpful comments. In the process of addressing these comments, we have performed supporting experiments and improved the presentation and clarity of the manuscript. Our detailed responses to the individual comments are shown below; quotations from the manuscript are shown with changes in bold. We give line numbers from the tracked-changes manuscript where appropriate.

Reviewer 1

1.1 This manuscript reports experiments, in which the evolution of brown carbon (BrC) aerosol upon exposure to OH is followed by the optical properties (scattering and absorption) at low (15%) and higher (60%) relative humidity. BrC aerosol was produced from the aqueous photooxidation of solutions containing resorcinol and H2O2, thus resembling aged biomass burning aerosol with high aromaticity. The results are that at 60% RH, oxidation of this BrC aerosol first induced an enhancement of absorption, followed by bleaching, with an inverse behavior observed for the single scattering albedo (SSA). At 15% RH, only a slowly increasing absorption was observed during the timescale of the experiments. Interpretation of the results is facilitated by a multilayer kinetics model, in which chemistry is lumped into a simple oxidation scheme involving one parent BrC leading to one second and one third generation oxidation product with differing optical properties. Comparison to experimental data in terms of optical properties, indicate that strongly contrasting diffusivity must be assumed between 15% RH and 60% RH to reproduce the experimental data. This allows speculating about different pathways of oligomerization and fragmentation to occur at various time periods. The evolution of BrC properties is a highly relevant topic of atmospheric aerosol chemistry due to ubiquitous presence of BrC compounds in a large variety of primary, aged primary or secondary organic aerosol.

The experiments seem to be well performed and carefully analyzed. Proper control experiments are performed to distinguish between photolysis and OH oxidation. Since the experiments are not accompanied by more detailed chemical analysis, the application of the kinetic model remains poorly constrained, though it provides a useful link between expected chemical processes and the optical properties, as they evolve under different humidity and thus likely differing diffusivity.

The manuscript is well written and structured; the conclusions are adequately supported by the experimental findings; and the kinetic model is presented and used with care and proper caveats. I recommend publication of this work with maybe just a few small revisions, following some specific comments below.

Thank you for these positive comments.

1.2 The model is based on chemical reactions just occurring at the surface, and the bulk only serves as a medium for reactants and products to diffuse; this seems reasonable for the reaction with OH. However, second generation oxidation may involve O2 or other reactive oxygen species deriving from the first and second step and may also proceed in the bulk. Of course, considering such would rapidly lead to more variables that would need to be tuned and would make the results more ambiguous. But maybe the authors could make an attempt in checking the sensitivity of the model results and parameters towards the experimental observables. I would also expect that O2 has quite different diffusivity than the large aromatic oligomers.

We agree that radical products of the initial OH reaction likely form RO_2 species by reaction with O_2. These RO_2 species may be converted to RO and initiate further oxidation of the brown carbon constituents or react with each other in a termination step. They may also facilitate auto-oxidation by causing hydrogen shifts. As the reviewer points out, an attempt to model these processes would introduce other parameters, such as the diffusion coefficient of O_2 in the particles and the absorptivities of any additional products, so we have not added them into our simple multi-phase model. However, we have modified the manuscript to discuss the potential role of RO_2 species in more detail. For example, RO_2 initiated reactions are suggested to contribute to uptake coefficients greater than unity at 60% RH. We have modified the text as follows:

- "**Processes other than directly OH-initiated oxidation also occur. For example, radical products of the initial OH reaction likely form RO2 species by reaction with O2. These RO2 species may react with each other in a termination step or react with NO, for example, to form RO (Richards-Henderson et al., 2015, 2016), which may initiate further oxidation of the brown carbon constituents. They may also facilitate auto-oxidation by abstracting hydrogen from adjacent groups on the same molecule. We do not consider these processes in our simple multi-phase kinetics model, since many other parameters, such as the diffusion coefficient of O2 in the particles and the absorptivities of any additional products, would have to be introduced, but they may play a role in the apparent values of uptake coefficients.**" (page 7, lines 20-26)

We take this opportunity to discuss a change to Figure 8. In the original manuscript, the modeled relative absorbance was compared to the inverse of the experimental relative single scattering albedo (SSA). Since the scattering coefficient appears in both the numerator and denominator of SSA and is much larger than the absorption coefficient, this comparison is problematic. To show the changing absorption properties of the particles more clearly, we now compare the modeled relative absorbance to the experimental absorption coefficient divided by that which would be expected if the initial complex refractive index (*m*) did not change during the experiment, accounting for size dependence. The experimental trends, shown in Figure R1, are also corrected for the contribution of photolysis.

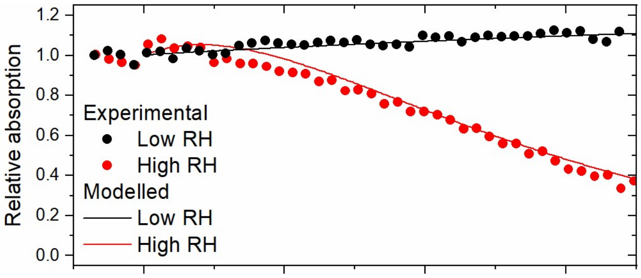

Figure R1. Experimental and modelled trends in relative absorption.

At 60% RH, the final value of the plotted quantity is about 0.40, rather than the value of 0.85 using the comparison plotted in the original Figure 8. To reproduce this trend – in particular, the more significant bleaching – the diffusion coefficient must be increased from 1 x 10^{-16} to 1 x 10^{-14} cm^2 s^{-1}, at which the particle is well-mixed, not semi-solid. The uptake coefficients and absorptivity were changed slightly, but do not alter the original discussion. At 15% RH, the diffusion coefficient was also increased by two orders of magnitude. At both RH conditions, the product C is set to be non-absorbing, but at 15% RH the uptake coefficient associated with its formation is set to only 0.1. The text was modified by substituting the new parameter values throughout. Other changes include the following:

- "**The parameters also suggest that, as RH decreases, reactivity decreases, and aerosol viscosity increases, such that particles are well-mixed at 60% RH but not at 15% RH**~~, and the aerosol is very viscous, even at 60% RH. At 15% RH, the aerosol will be viscous enough to confine products of fragmentation, leading to their recombination, such that little bleaching is observed on the experimental timescale~~." (page 1, lines 19-22)

- "**This modelled relative absorption is compared to the to the experimental absorption coefficient normalized to that which would be expected if the initial complex refractive index (*m*) did not change during the experiment, accounting for size dependence. Experimental times series of this normalized absorption were derived for photolysis and heterogeneous OH oxidation experiments, and the latter were corrected for the effect of photolysis.** ~~During heterogeneous OH oxidation, the evolution of the SSA of the particles incorporates changes in both absorption and scattering. However, the changes in absorption are likely dominant. For example, for fixed values of n (1.35) and particle diameter (200 nm), a 50% decrease in k (from 0.04 to 0.02) gives a 10% increase in Qsca but almost a 50% decrease in Qabs. Consequently, we assume that Qsca is steady, and we compare the modelled trends in relative absorption to the experimental trends in the inverse of relative SSA.~~" (page 7, lines 11-19)

- We find that the observed trend in relative absorption at 60% RH – **in particular, the significant bleaching** – can~~not~~ be reproduced **only** if the aging particles are taken as well-mixed**, so diffusion of A from the bulk to the surface is not restricted**~~; if $D_{b,i}$ is taken as 1 x 10^{-14} cm^2 s^{-1}, the decay in the concentration of A is about the same in all three bulk layers (see Fig. S6a), and the abrupt cessation of absorption enhancement cannot be captured. As shown in Fig. S7, if the absorptivities are fixed, and the uptake coefficient is scanned from 0.2 to 10, the trends in relative absorption have the same shape (simply stretched or compressed along the time axis), because the particles are well-mixed. On the other hand, if $D_{b,i}$ is taken as 1 x 10^{-16} cm^2 s^{-1}, the fraction of species A at the surface decays faster than in the bulk (see Fig. S6c), the modelled trends cannot be superimposed by scaling along the time axis (see Fig. S8), and the abrupt cessation of absorption enhancement to be captured~~." (page 12, lines 8-15)

- "**Though the extent of bleaching is captured by the model, and rapid initial colour enhancement is not. We speculate the other processes, like auto-oxidation, could contribute to this feature**." (page 12, lines 20-22)

1.3 The estimated diffusivity at 60% RH and also the fact that diffusion limitations are so apparent are a bit surprising. The authors are explaining it with the high aromatic content and the ease with which aromatic oligomers are formed. Can the hygroscopic growth be estimated from the experiment between 15% and 60% RH. The lack of significant water uptake could support the semi-solid character of these particles at 60% RH.

As described above, the modelled diffusion coefficient at 60% RH increased by two orders of magnitude, upon comparing the modelled relative absorbance to the experimental absorption coefficient divided by that which would be expected of a constant refractive index. Consequently, the particles are no longer estimated to be semi-solid at 60% RH.

Nonetheless, we agree that it would be informative to roughly estimate the extent of hygroscopic growth at 60% RH. Unfortunately, the initial size distributions vary between experiments, including replicates at the same RH, so we cannot directly compare the 15 and 60% RH experiments to evaluate hygroscopic growth at 60% RH.

To address this issue, we performed an additional experiment, in which BrC particles were sampled from the chamber alternately with and without a diffusion dryer upstream of the DMA. The conditioning was alternated every 15 min, allowing time for the RH of the sheath flow to stabilize. As shown in Figure R2 (also Figure S5 in the supporting information), the size distribution slowly shifts to larger mobility diameters, because smaller particles are lost faster than larger particles. Besides this trend, the variation between the conditions appears to be negligible, so there is not significant water uptake. Nonetheless, slight differences in scattering coefficients of nascent and dried particles are observed, as described in our reply to comment 2.3.

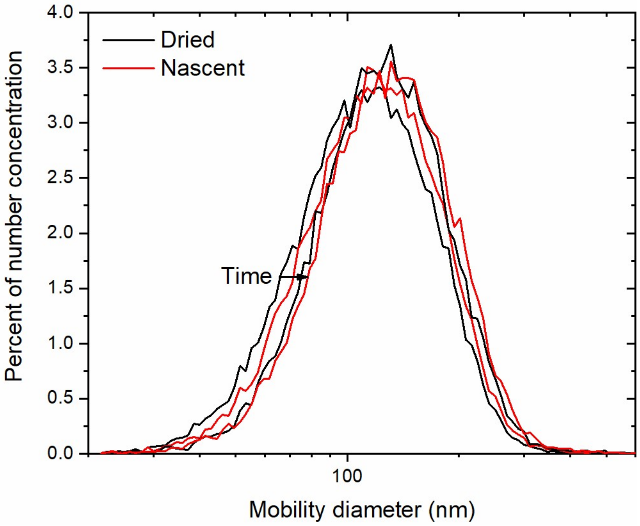

Figure R2. Size distributions of dried and nascent particles, collected alternately in 15 min intervals.

The manuscript was modified as follows:

- "**In one experiment, BrC particles were sampled from the chamber alternately with and without a diffusion dryer upstream of the DMA. The conditioning was alternated every 15 min, allowing time for the RH of the sheath flow to stabilize. As shown in Fig. S6, the size distribution slowly shifts to larger mobility diameters, because smaller particles are lost faster than larger particles. Besides this trend, the variation between the conditions appears to be negligible, so there is not significant water uptake at 60% RH.**" (page 9, lines 6-10)

1.4 Based on the reported results, under the conditions of the experiments, OH oxidation dominated the changes in optical properties in comparison to pure photolysis alone. Could the authors try estimating the relative impact of photolysis and OH under atmospheric conditions. Photolysis of BrC or reactions of their triplet excited states may also lead to later generation radical processes, similar to those initiated by OH; therefore the relative impact of OH versus that of BrC induced photochemistry on aerosol aging may require some attention.

This is a very important issue, and we now address it in the text as follows:

- "The emission of the UV-B black-lights in the chamber**, with a peak at 310 nm,** is not representative of natural sunlight, so we do not draw direct comparisons between the timescale of our experiments and that of photolysis in the atmosphere. Rather, we performed photolysis experiments to account for the effects of photolysis during the heterogeneous OH oxidation experiments. **Wong et al. (2015) have shown that for this chamber equipped with UV-B bulbs, the photo flux at wavelengths below 310 nm is much greater than for a clear-sky summer day; for example, at 300 nm, the photon flux from the bulbs is close to its peak value of about 1×10^{14} photons s^{-1} cm^{-2} nm^{-1}, while the photon flux outside is negligible. Light at wavelengths below 310 nm is likely driving most of the photo-chemistry during the photolysis experiments, so we believe the relative impact of photolysis would be small in the atmosphere, even considering that the ambient OH concentration is lower than in the chamber.**" (page 9, lines 13-21)

Reviewer 2

2.1 Overall, I find this to be an interesting study that looks at how photochemical aging influences the absorptivity of aqueous, secondary brown carbon. The results and interpretation, if correct, are a useful contribution to the literature. I do, however, have two substantial concerns. (i) The photoacoustic method has been experimentally shown to have potential negative biases at elevated RH, despite the references given. (The authors missed a critical reference.) (ii) It is, at times, difficult to understand exactly what conditions were run for the optimized modeling, and thus it was a little difficult to fully understand the interpretation provided. A table and further description may be helpful.

We agree that these are substantial concerns. To address the possibility of negative bias at 60% RH, we have performed a supporting experiment, described in detail in our reply to comment 2.3. We have added the critical reference to the manuscript. We have also modified and clarified our discussion of the modeling results, as described in our replies to comments 1.2 and 2.8-2.10.

2.2 Abstract: It would be good to explicitly state that this study investigates heterogeneous processing of "aqueous, secondary BrC" or something like that, to distinguish from primary BrC.

Done.

2.3 I am concerned that there is a potentially fatal flaw in this study at least with respect to a portion of the data. It may be that there is not, but this needs to be addressed. The authors made some of their absorption measurements with their PAS instrument at elevated RH. They cite two studies saying that they "assume there is no evaporation of water ..." and given two citations, both theoretical. Unfortunately, much more recent experimental evidence has developed that suggests that there can be negative biases that result from evaporation of water vapor. The key paper is by Langridge et al. (AS&T, 2013). The authors do not cite this paper, which is an unfortunate oversight. Unless the authors can demonstrate that their measurements at elevated RH are not impacted by evaporation of water vapor. The apparent bleaching that is observed here could, potentially, simply be a reflection of the particles becoming more hygroscopic upon oxidation, and thus there being a negative bias of increasing magnitude. I believe it is up to the authors to demonstrate that their results are not biased by evaporation effects. If they cannot, then the 60% RH observations should probably be removed.

The reviewer suggests that the particles may become more hygroscopic during oxidation, leading to more water uptake and, upon irradiation in the photo-acoustic spectrometer, water evaporation from the particles. Through evaporation, some of the energy of the absorbed photons would be lost without contributing to the detected pressure wave. In addition to this instrumental artifact, progressively more water uptake could lead to genuinely greater scattering coefficients, which would also result in apparent bleaching.

To address these concerns, we performed an additional photo-oxidation experiment. Particles were sampled from the chamber to the photo-acoustic spectrometer and scanning mobility particle spectrometer, alternately with and without a diffusion dryer downstream of the chamber. Results of this experiment are illustrated in Figures R2-R3 and the supporting information (Figures S7 and S8 in the supporting information). We note that this experiment was conducted in a different chamber than the original experiments, so some of the conditions (like average OH concentration) may differ. Unlike in the original experiments, some particle growth occurred, leading to a significant increase in the scattering coefficient.

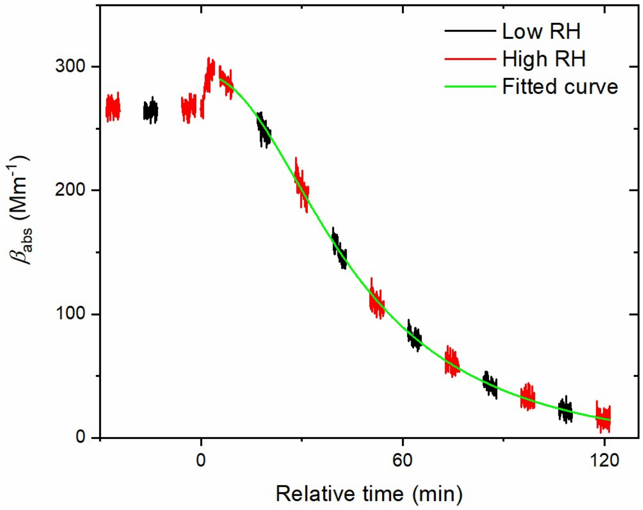

Figure R3. Time series of the absorption coefficient at 405 nm for dried (low RH) and nascent (high RH) particles, measured by alternatively sending the particle flow through a diffusion dryer.

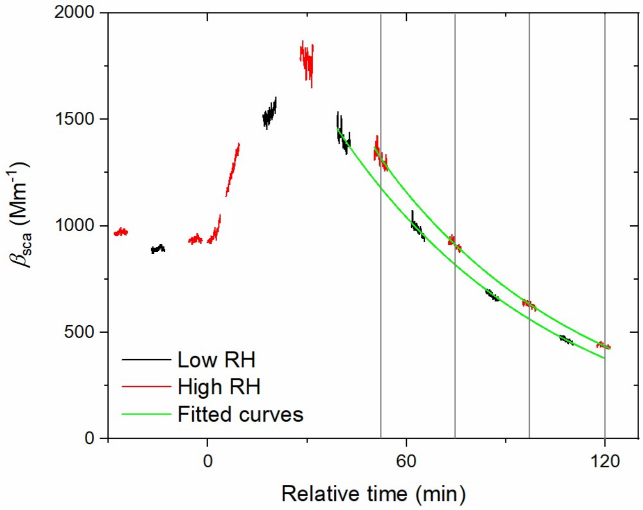

Figure R4. Time series of the scattering coefficient at 405 nm for dried (low RH) and nascent (high RH) particles.

Nonetheless, the trends in absorption and scattering coefficients demonstrate that the results of the original experiments are valid. First, as shown in Figure R3, the decrease in the absorption coefficient following the initial colour enhancement can be well represented by fitting a single logistic function to measurements for both nascent and dried particles. In other words, there is not a significant negative bias from water evaporation. Second, as shown in Figure R4, the relative difference between the scattering coefficients of the nascent and dried particles, based on fitting exponential functions to the measurements after the initial particle growth, is roughly constant across four reaction time intervals from about 50 to 120 min: 11, 10, 11, and 13%. This consistency indicates that the particles are not taking up significantly more water as they react with OH.

We have modified the text as follows:

- "**One potential source of bias in photo-acoustic measurements is evaporation of water from particles (Baker, 1976; Raspet et al., 2003; Langridge et al., 2013); through evaporation, some of the energy of the absorbed photons may be lost and not contribute to the detected pressure wave. On this basis, the higher RH was selected to be lower than the maximum operating RH of the PASS (70%). To verify that evaporation of water did not influence the measurements of absorption coefficients, we alternately sampled with and without a diffusion dryer downstream the chamber in one experiment.**" (page 5, lines 26-30)

- "**As described above, evaporation of water from particles can result in a negative bias in photo-acoustic measurements Langridge et al., 2013). If heterogeneous OH oxidation significantly increased the hygroscopicity of the particles, the water content of the aerosol would increase during the experiment. The resulting increase in the magnitude of the bias could contribute to apparent bleaching. In addition to this instrumental artifact, progressively more water uptake could lead to genuinely greater scattering coefficients, which would also result in apparent bleaching. We investigated these potential effects by alternately sampling with and without a diffusion dryer downstream of the chamber at 60% RH. As shown in Fig. S7, the absorption coefficient does not depend on the conditioning. The scattering coefficient is about 10% lower for the dried particles (see Fig. S8), but this difference is roughly steady during photo-oxidation. In other words, the particles do not become significantly more hygroscopic, and the changes in absorption and scattering coefficients are indeed due to the chemical evolution of the particles.**" (page 11, lines 1-10)

We thank the reviewer for bringing the paper by Langridge et al. to our attention; we now cite this paper, along with the earlier theoretical papers.

2.4 Abstract: Regarding the conclusion that at 15% RH the particles are viscous enough to "confine products of fragmentation," if the products are confined, how does the OH reach these molecules in the first place to react with them? The high viscosity would similarly cause the reactions to occur primarily at the surface, correct? And if so, the products would be in a very good spot for evaporation.

Under the conditions originally proposed for 15% RH – specifically, the very small diffusion coefficient of 1 x 10^{-18} cm^2 s^{-1} – the model products B and C, which form at the surface, do not diffuse appreciably. Even after 180 min, their concentrations in bulk layer 3 are negligible. This observation was the basis of our conclusion that the products are strictly confined to the surface. We agree that the products of fragmentation (i.e., species C) likely evaporate from the particle surface to some extent. In fact, the size distributions at 15% RH shift slightly to smaller sizes at later OH exposures. Since we now assume a larger diffusion coefficient of 1 x 10^{-16} cm^2 s^{-1}, as described in our reply to comment 1.2, we have removed the suggestion that recombination may occur, as follows:

- “~~This equivalence may indicate that, if fragmentation occurs due to reaction of OH with B, the strict confinement of the fragments leads to recombination, such that the absorption persists.~~ It is ~~also~~ possible that ~~stable~~ fragmentation products ~~form, but they~~ volatilize out of the condensed phase to a ~~much~~ greater extent than they diffuse to the bulk phase, because the particles are so viscous~~; in this case, the decreased molar absorptivity of the products would have little effect on the total particle absorption~~. In fact, a slight decrease in the mean geometric surface diameter suggests that there is some degree of volatilization.” (page 13, lines 6-11)

2.5 P8/L11: Was only the SSA matched, or were the absolute absorption and scattering also matched during the RI determination? If only the SSA, how can the authors ensure that they have a unique solution? There are a multitude of combinations of n and k that can give the same SSA value. Especially given that the n value determined differs so much from other SOA types.

SSA, rather than the absolute absorption and scattering coefficients, was used to derive an approximate complex refractive index (*m*). In the deposition experiment, the aerosol is unperturbed, so *m* is assumed to be constant, while the aerosol distribution and SSA change slightly. We agree that any reasonable combination of *n* and *k* can give good agreement for an individual distribution, but it cannot reproduce the observed trend in SSA, as shown in Figure R5 and the supporting information (Figure S4).

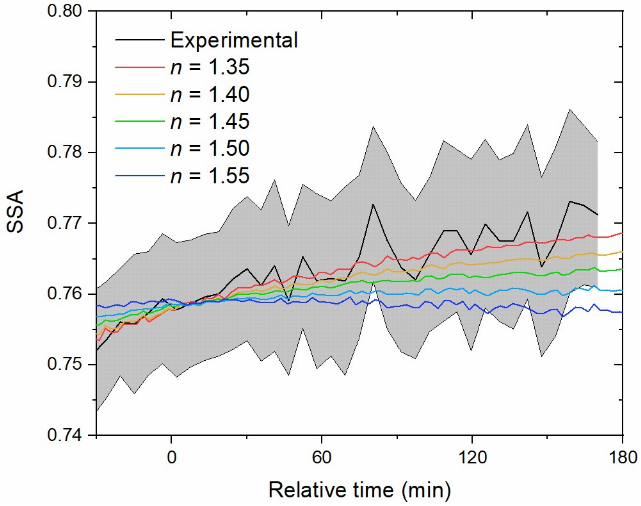

Figure R5. Time series of observed and predicted (based on the size distributions) SSA during a deposition experiment.

We agree that it would be preferable to use the absolute absorption and scattering coefficients. However, we find that the coefficients predicted from the distributions are lower than those observed for all values of *m*. Unfortunately, the impactor installed in the DMA had an orifice of 0.0502 cm, but the value was set to 0.0708 cm in the firmware, so the flow rate on the DMA display was too high. As a result, the particles were diluted more than expected before reaching the CPC, leading to lower number and cross sectional area concentrations.

We stress that, here, even an approximate value of the *m* is adequate to distinguish changes in the SSA due to changes in the size distribution from those in the chemical composition. For all assumed *m* values, for example, the sudden colour enhancement and significant bleaching observed at 60% RH is not predicted, so it must be due to chemical evolution.

The manuscript was modified as follows:

- "**Stepping *n* from 1.40 to 1.55 and adjusting *k* accordingly demonstrates that the good agreement for this refractive index is unique, as shown in Fig. S9. We stress that even an approximate value of the refractive index is adequate to distinguish whether changes in the SSA are due to changes in the size distribution or chemical composition.**" (page 8, line 33-page 9, line 1)

2.6 P9/L24: Presumably, a difference between 0.040 and 0.041 are within experimental uncertainty.

We agree that such a small difference in *k* is within the experimental uncertainty; nonetheless, the respective values give the best agreement with the average values of SSA. We modify the text, acknowledging the values are similar:

- "The initial geometric mean surface diameter was slightly higher than in the photolysis experiment described above (about 196 nm compared to 160 nm), so although the initial aerosol was slightly more scattering (higher SSA), the value of k required to reproduce the SSA before irradiation is ~~slightly higher~~ **very similar** (0.041 compared to 0.040)." (page 10, lines 24-27)

2.7 P10/L3: it would be helpful if the authors could clarify what they mean when they say they "observed uniform bleaching." Also, the origin of the red curve in Fig. S5 is a bit unclear, if it does assume a constant n and k.

We apologize for a mistake in the legend of the original Figure S5b: the labels for the red and black curves were swapped. Assuming constant values of *n* and *k* gives the relatively steady predicted curve shown in black. The observed uniform bleaching is evident, beginning at relative time zero, coincident with the cusp of the red curve. The labels have been corrected.

2.8 P10/L21: How large of a MW would be necessary to yield a gamma = 1?

With the current set of parameters for 60% RH, decreasing the uptake coefficient for the initial BrC (i.e., species B) from 5.0 to 1.0 requires increasing the molecular weight from 326 to 1600 g mol^{-1}, in order to reproduce the experimental trend in relative absorption. We modify the text as follows:

- "**Scaling the uptake coefficients such that $\gamma_{OH,A}$ decreases from 5.0 to 1.0 requires increasing the molecular weight from 326 to 1600 g mol^{-1}. It is difficult to**

> **rationalize such large oligomers forming during the 4-h aqueous photo-oxidation, so secondary radicals are indeed likely contributing to oxidation.**" (page 12, lines 1-3)

2.9 Fig. 8: This figure could probably benefit from additional panels showing the time-evolution of the normalized concentrations of A, B and C. It is difficult to visualize in the model how there is a sudden turnover that occurs with the 60% RH experiment with only two products and a continuous evolution. It would seem, at least to me, that some step change is necessary and the origin of this is not abundantly clear from the text.

> We have added two panels to Figure 8, shown below as Figure R6, one for each RH condition. In each, 12 time series are plotted, one for each species in each layer. As shown in the middle panel, the concentrations of the individual species are the same in all four layers at 60% RH; in other words, the particles are well-mixed. In contrast, as shown in the bottom panel, the concentrations of the individual species vary significantly across the layers at 15% RH.

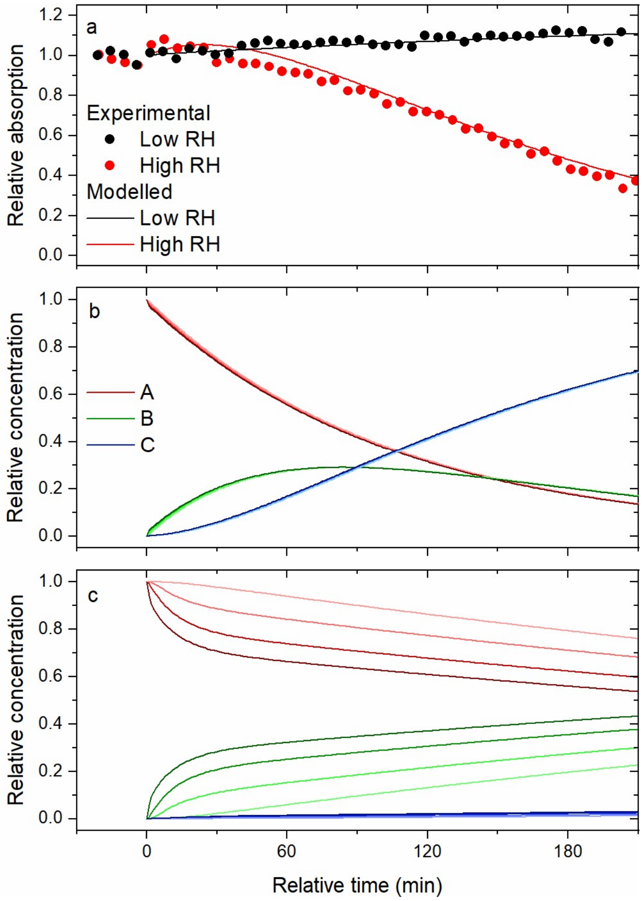

> Figure R6. Time series of (a) observed and modelled relative absorption at 60 and 15% RH and the modelled relative concentrations of A, B, and C at (b) 60 and (c) 15% RH. The curves are shaded according to layer, with the darkest curves corresponding to the surface layer.

The text was modified as follows:

- "**As shown in Fig. 8b, the concentrations of A, B, and C are the same in all four layers.**" (page 12, line 14)

- "On a related note, because the viscosity is so high, the products B and C are much more concentrated at the surface than in the bulk layers (see Fig. ~~9~~ **8c**). Consequently, at 15% RH, the ~~aged~~ **aging** particles likely **consist of less absorbing cores and highly absorbing shells** ~~consist of unchanged BrC cores encased in thin, more absorptive shells~~." (page 13, lines 11-14)

2.10 Figures S7/8/9/etc.: It would be very useful if the authors would report the epsilon values assumed for each of these simulations in the caption. It is difficult to understand whether the differences between e.g. Fig. S8 and S9 are the result of differences in the diffisivity alone, or because different assumptions have been made about the evolution of the absorptivity and the absorptivity of the products. I say this because the authors could do a better job of explaining how the evolution of the product species differs between the 60% RH and 15% RH cases, given that they show that at 60% RH the particles are already fairly viscous, with differential oxidation between the surface layers and the bulk. What happens if all the authors do is drop the diffusivity from 10^-16 (which worked for RH = 60%) to 10^-18, keeping everything else the same? Perhaps this is what Fig. S8 and Fig. S9a are showing, but it is not abundantly clear as written and presented. And I actually think that these figures fundamentally differ in what is assumed about the absorptivity of the products.

To generate these figures, ε_B was set to 2.5, and ε_B was set to either zero or 2.5, as well. These are the same conditions that were used to give the original model results in Figure 8, so the supporting figures do not fundamentally differ from what was described about the absorptivities of the products in the text.

However, Figures S7-S9 were intended to illustrate how a low diffusion coefficient was required in the model even at 60% RH. Comparing the modeled relative absorption to the experimental absorption coefficient divided by that which would be expected of a constant refractive index resulted in different values for the model parameters, as described in our reply to comment 1.2. In particular, the diffusion coefficient increased by two orders of magnitude, required to reproduce the significant bleaching. Consequently, we have decided to omit the original Figures S7-S9 from the revised manuscript.

2.11 P12/L16: it might be good to indicate that Sumlin investigated only a handful of biomass sources.

We have modified the text as follows:

- "Recently, Sumlin et al. (2017) observed bleaching due to heterogeneous OH oxidation of primary BrC derived from ~~biomass~~ burning **of a number of types of biomass fuels**, which lost almost 50% of its absorption at 375 and 405 nm after the equivalent of about 4.5 days in the atmosphere." (page 14, line 5)

Heterogeneous OH oxidation of secondary brown carbon aerosol

Elijah G. Schnitzler, Jonathan P. D. Abbatt

Department of Chemistry, University of Toronto, Toronto, ON, M5S 3H6, Canada

Correspondence to: Jonathan P. D. Abbatt (jabbatt@chem.utoronto.ca)

Abstract. Light-absorbing organic aerosol, or brown carbon (BrC), has significant but poorly-constrained effects on climate; for example, oxidation in the atmosphere may alter its optical properties, leading to absorption enhancement or bleaching. Here, we investigate for the first time the effects of heterogeneous OH oxidation on the optical properties of a laboratory surrogate of aqueous, secondary BrC in a series of photo-oxidation chamber experiments. The BrC surrogate was generated from aqueous resorcinol, or 1,3-dihydroxybenzene, and H_2O_2 exposed to >300 nm radiation, atomized, passed through trace gas denuders, and injected into the chamber, which was conditioned to either 15 or 60% relative humidity (RH). Aerosol absorption and scattering coefficients and single scattering albedo (SSA) at 405 nm were measured using a photo-acoustic spectrometer. At 60% RH, upon OH exposure, absorption first increased, and the SSA decreased sharply. Subsequently, absorption decreased faster than scattering, and SSA increased gradually. Comparisons to the modelled trend in SSA, based on Mie theory calculations, confirm that the observed trend is due to chemical evolution, rather than slight changes in particle size. The initial absorption enhancement is likely due to molecular functionalization and/or oligomerization, and the bleaching to fragmentation. By contrast, at 15% RH, slow absorption enhancement was observed, without appreciable bleaching. A multi-layer kinetics model, consisting of two surface reactions in series, was constructed to provide further insights regarding the RH-dependence of the optical evolution. Candidate parameters suggest that the oxidation is efficient, with uptake coefficients on the order of unity. The parameters also suggest that, as RH decreases, reactivity decreases, and aerosol viscosity increases, such that particles are well-mixed at 60% RH but not at 15% RH~~, and the aerosol is very viscous, even at 60% RH. At 15% RH, the aerosol will be viscous enough to confine products of fragmentation, leading to their recombination, such that little bleaching is observed on the experimental timescale~~. These results further the current understanding of the complex processing of BrC that may occur in the atmosphere.

1 Introduction

Among all atmospheric constituents, aerosols have the most uncertain radiative forcing, partly due to an incomplete understanding of carbonaceous aerosols (Chung et al., 2012). In particular, the climate effects of light-absorbing organic aerosol, or brown carbon (BrC) (Bond, 2001; Kirchstetter et al., 2004), are poorly constrained, compared to those of elemental black carbon (BC) (Ramanathan and Carmichael, 2008).

One source of this uncertainty is the wide range of sources of BrC (Laskin et al., 2015). Low-temperature biomass burning results in the formation of primary BrC (Bahadur et al., 2012; Chen and Bond, 2010; Lewis et al., 2008; Radney et al., 2017). Many classes of compounds, including nitro-aromatics, polyphenols, and substituted polycyclic aromatic hydrocarbons (Lin et al., 2016), have been identified in primary BrC, but their concentrations and absorptivities vary significantly. At a site strongly influenced by biomass burning in Germany, the contribution of nitro-aromatics to the absorption of 370 nm light by BrC was roughly 1 % (Teich et al., 2017); in contrast, in a field campaign in Israel, during a bonfire festival, the contribution of nitro-aromatics to the total absorption of >400 nm light was greater than 50 % (Lin et al., 2017), in good agreement with results from controlled burns during the fourth Fire Lab at Missoula Experiment (Lin et al., 2016). In recent applications of size-exclusion chromatography, BrC constituents with molecular masses across the range of 10^2–10^4 Da have been observed (Di Lorenzo et al., 2017; Di Lorenzo and Young, 2016; Wong et al., 2017). Larger, oligomeric compounds (> 1000 Da) have been observed to contribute most of the absorbance (Di Lorenzo and Young, 2016). If the primary BrC particles subsequently pass through a high-temperature region of biomass burning (Tóth et al., 2014), they may form tar balls (Chakrabarty et al., 2010; Hoffer et al., 2016), which are significantly more absorptive (Alexander et al., 2008).

BrC may also form from secondary processes. For example, ozonolysis of catechol and guaiacol, abundant emissions from biomass burning (Schauer et al., 2001), in the gas phase leads to the formation of lower-volatility products that partition into the condensed phase to form secondary organic aerosol (SOA) that is light-absorbing (Ofner et al., 2011). Light-absorbing SOA has also been observed to form from the gas-phase photo-oxidation of other precursors: e.g., naphthalene (Lambe et al., 2013; Lee et al., 2014). In a recent field campaign, reactions in the condensed phase of cloud droplets or aqueous aerosols have also been shown to result in the formation of light-absorbing SOA (Gilardoni et al., 2016). In the laboratory, heterogeneous oxidation of catechol has been studied at air–solid (Pillar et al., 2015) and air–water (Pillar et al., 2014; Pillar and Guzman, 2017) interfaces; at the air–water interface, functionalization, leading to polyphenols and hydroxylated quinones that are expected to be highly-absorptive, followed by fragmentation was observed (Pillar and Guzman, 2017). Heterogeneous reactions are sensitive to particle diameter, so they may in part be responsible for the observation of higher concentrations of BrC in particles in the accumulation mode than in the coarse mode (Liu et al., 2013). Reactions of nitrogen-containing species (e.g., ammonium sulfate and methylamine) with aldehydes (e.g., glyoxal and methyglyoxal) have also been shown to result in BrC (De Haan et al., 2009, 2011; Lee et al., 2013; Yu et al., 2011). Furthermore, the formation of intra- or inter-molecular charge transfer complexes, similar to what has been proposed to occur in natural waters (Del Vecchio and Blough, 2004), may enhance the absorption of BrC (Phillips and Smith, 2014, 2015; Rincón et al., 2009).

In addition to the wide range of classes of BrC, the evolution of BrC upon atmospheric aging contributes to the uncertainty in its climate forcing. During the lifetime of the particles or cloud droplets, BrC constituents are photolyzed or react with oxidants; the resulting chemical evolution leads to evolution of the optical properties of the aerosol. Field measurements have demonstrated that the absorption by BrC may decay drastically during transport, although a small fraction may be recalcitrant (Forrister et al., 2015). On the other hand, in a recent field campaign, absorption at 365 nm by BrC was the same in a fresh convective storm outflow and its one-day-aged plume, suggesting either that photo-bleaching was minimal or that secondary chemistry produced new chromophores that compensated for any photo-bleaching (Zhang et al., 2017).

In the laboratory, the evolution of absorption induced by photolysis and oxidation has been observed for a variety of BrC surrogates in the solution phase, including extracts of biomass burning BrC (Lin et al., 2016; Wong et al., 2017), extracts of SOA derived from naphthalene under high-NO_x conditions (Lee et al., 2014), products of (methyl)glyoxal and ammonium sulfate (Wong et al., 2017; Zhao et al., 2015), products of pyruvic acid polymerization (Rincón et al., 2009), and nitrophenols (Zhao et al., 2015). Fewer studies have investigated the evolution of BrC aerosol upon photolysis and heterogeneous oxidation. Aging of particle and gas emissions from biomass burning results in formation of BrC or non-absorbing SOA coatings on BC particles, leading to enhanced absorption (Saleh et al., 2013; Tasoglou et al., 2017). In flow-tube experiments, BrC aerosol from atomized methylglyoxal and ammonium sulfate has been shown to increase in absorptivity upon exposure to ozone, due to carbonyl products (Sareen et al., 2013). BrC from biomass burning exposed to natural sunlight has been shown to photo-bleach; additionally, the rate of photo-bleaching decreased in the presence of NO_x, possibly due to formation of secondary BrC constituents that slightly compensate for photo-bleaching (Zhong and Jang, 2014). Most recently, in potential aerosol mass reactor experiments, primary BrC from biomass burning exposed to irradiation, ozone, and hydroxyl radical (OH) has been shown to lose almost 50% of its absorption at 375 and 405 nm after the equivalence of 4.5 days of residence time in the atmosphere (Sumlin et al., 2017).

Here, we consider the fate of secondary BrC constituents from cloud processing upon droplet evaporation and subsequent exposure to OH radicals. The first question to raise is whether the optical properties of secondary BrC aerosol evolve at atmospherically-relevant OH exposures; another broad question is whether this evolution is dependent on relative humidity (RH). To address these questions, we investigate for the first time the heterogeneous OH oxidation of a secondary BrC surrogate aerosol, generated from the product mixture of aqueous OH oxidation of resorcinol, or 1,3-dihydroxybenzene. Experiments were conducted in a 1-m^3 photo-oxidation chamber at 15 and 60% RH, and aerosol absorption, scattering, and single scattering albedo (SSA) at 405 nm were measured *in situ* using a photo-acoustic spectrometer with an integrated reciprocal nephelometer. Changes in the optical properties were observed, raising another question, whether these changes were due to the chemical evolution of the particles or simply slight changes in the size distributions. Mie theory calculations were used to demonstrate that these changes were due to the evolution of the chemical composition and, in turn, the complex refractive index of the particles. A final question is whether the features observed for the evolution of optical properties at each RH can be reproduced by a simple kinetics model. Consequently, a multi-layer kinetics model was constructed, and potential parameters are proposed.

2 Methods

2.1 Experimental methods

2.1.1 Preparation of BrC surrogate by aqueous OH oxidation

The BrC surrogate was prepared by aqueous OH oxidation of resorcinol. An aqueous solution of 10 mM resorcinol and 10 mM H_2O_2 was prepared and placed in a cylindrical photochemical reactor (Rayonet, RPR-200), where it was irradiated with UV-B blacklights (Ushio, G8T5E) with peak emission at 306 nm. The reactor is equipped with a cooling fan and magnetic stirrer. The solution was housed in a glass bottle, so it was not exposed to light with wavelengths <300 nm. The solution was irradiated for 4 h, resulting in an orange product mixture. When H_2O_2 was not added to solution, no colouration was observed in the same period of irradiation. UV-vis spectra were measured by passing light from a broadband source, with coupled deuterium and tungsten halogen lamps (Ocean Optics, DT-Mini-2), through a 1-cm quartz cuvette to a grating-based UV-vis spectrometer (Ocean Optics, USB2000+ UV-VIS-ES). Each solution was prepared with deionized water (18 mΩ cm), and the pH was not adjusted. After irradiation, the solution was atomized immediately to inject BrC aerosol into the chamber. A fresh solution was prepared for each chamber experiment.

2.1.2 Preparation of yellow dye aerosol

Heterogeneous OH oxidation of a yellow azo dye, Cibacron Brilliant Yellow 3G-P (CBY; Sigma), was also investigated. The dye has a high molecular mass, 831.02 g mol^{-1}, so it is non-volatile, and it contains sulfonate groups, so it is hygroscopic, similar to Solvent Black 5, which is commonly used in calibrations of aerosol optical instruments (Bluvshtein et al., 2017; Lack et al., 2006; Wiegand et al., 2014). CBY aerosol was prepared by atomizing 1 mM CBY solutions. The absorption spectrum of a diluted solution is shown in Fig. S1. Peak absorbance occurs at 404 nm.

2.1.3 Heterogeneous OH oxidation of BrC surrogate aerosol

The experimental setup during heterogeneous OH oxidation is illustrated in Fig. 1. The aqueous solutions of BrC surrogate were aerosolized using a constant output atomizer (TSI, 3076). To obtain appreciable aerosol absorption, it was necessary to atomize for roughly 3 h, and during this time the resorcinol product solution became significantly more absorbing. Since particles injected at the end of this period may be more absorbing than those injected at the beginning, the absorption and scattering coefficients must be qualified as time-integrated properties. Two denuders consisting of tubular mesh packed in granular activated carbon were placed in series downstream of the atomizer to remove trace gases. In preliminary experiments without the denuders in place, significant particle growth occurred upon exposure to OH, due to gas phase photo-oxidation of volatile species in the resorcinol product mixture, increasing the scattering of the aerosol. (In the yellow dye experiments, the activated carbon denuders were not used, because the large dye did not partition out of the aerosol phase following atomization, and no particle growth occurred.)

The aerosol was then injected into the Mobile Oxidative Chamber for Aging (MOCA), which has been described in the past (Wong et al., 2015). Briefly, the chamber consists of a 1-m^3 bag composed of fluorinated ethylene propylene (FEP) film surrounded by an array of 24 UV-B blacklights (Philips, TL 40W/12 RS) with peak emission at 310 nm. Experiments were conducted at roughly 15 or 60% RH. Before each experiment, the chamber was cleaned by bubbling air through H_2O_2 (Sigma, 30% w/w in water) at about 12 L min^{-1} and irradiating the chamber for at least 12 h. About 6 h before the start of each experiment, the chamber was flushed with either dry or humidified air at 12 L min^{-1}, to achieve 15 or 60% RH, respectively. Temperature and RH were measured in the chamber using a capacitance probe (Vaisala, HMP75B). Air was supplied by a clean air generator (Aadco, 737).

During and after particle injection, aerosol size distributions were monitored using a scanning mobility particle sizer (SMPS), consisting of a differential mobility analyzer (DMA; TSI, 3081) and a condensational particle counter (CPC; TSI, 3772). The sample flow rate of the CPC is 1 L min^{-1}, but only 0.3 L min^{-1} was sampled through the DMA; the difference was sampled through a filter. The DMA sheath flow rate was set to 3 L min^{-1}.

Aerosol absorption and scattering were measured using a photo-acoustic spectrometer (DMT, PASS), equipped with 405 and 781 nm lasers and a reciprocal integrating nephelometer (Sharma et al., 2013) with a low truncation angle (Abu-Rahmah et al., 2006). Absorption and scattering coefficients were taken as averages of 120 samples, each with an integration time of 2 s. Acoustic and zero calibrations, the latter consisting of 30 samples, were performed before each average, so the interval between averaged coefficients was 5 min. The zero calibrations account for slight changes in the gas phase background – in particular, water vapour. ~~The higher RH was selected to be lower than the maximum operating RH of the PASS (70%). We assume that there is no evaporation of water or organic components of the particles due to absorption (Baker, 1976; Raspet et al., 2003).~~ In the following discussion, we characterize the optical properties of the aerosol in terms of the directly-measured absorption and scattering coefficients ($\beta_{\rm abs}$ and $\beta_{\rm sca}$) and the single scattering albedo (SSA = $\beta_{\rm sca}/[\beta_{\rm abs} + \beta_{\rm sca}]$). Relative SSA is calculated by taking the ratio of the current and initial values; e.g., SSA/SSA$_0$.

Following aerosol injection, the size distribution and optical properties of the BrC aerosol were monitored for about 1 h before passing air through a glass bubbler containing H_2O_2 into the chamber at a flow rate of 1.5 L min^{-1}. Following 1 h of bubbling, the blacklights were turned on to produce OH from the photolysis of H_2O_2. Oxidation was monitored for about 3 h.

One potential source of bias in photo-acoustic measurements is evaporation of water from particles (Baker, 1976; Raspet et al., 2003; Langridge et al., 2013); through evaporation, some of the energy of the absorbed photons may be lost and not contribute to the detected pressure wave. On this basis, ~~T~~the higher RH was selected to be lower than the maximum operating RH of the PASS (70%). To verify that evaporation of water did not influence the measurements of absorption coefficients, we alternately sampled with and without a diffusion dryer downstream of the chamber in one experiment.

2.1.4 Determination of OH concentration

In a separate set of high-RH experiments, *o*-xylene (Sigma, ≥98%) was injected into the chamber as a tracer for OH, following the aerosol injection. The concentration of the tracer was measured using a proton-transfer-reaction mass spectrometer (PTR-

MS; Ionicon). Following injection of *o*-xylene, air was bubbled through H_2O_2 into the chamber at 1.5 L min^{-1} for 1 h; subsequently, the blacklights were turned on to initiate photo-oxidation. The concentration decayed exponentially, due to dilution and pseudo-first-order reaction with OH. Dividing the experimental reaction rate constant by the second-order reaction rate constant (Atkinson and Arey, 2003) gave a steady-state OH concentration of (1.6 ± 0.2) x 10^{7} molecule cm^{-3}. Three experiments were performed with different initial *o*-xylene concentrations to verify that the tracer did not contribute significantly to the total OH sink; i.e., the steady-state OH concentration did not systematically increase as the *o*-xylene concentration decreased. The tracer could not be added to all experiments, because the photo-oxidation products partitioned onto the pre-existing particles to form secondary organic aerosol (SOA), which drastically increased the scattering coefficient. The average OH concentration is used to present results in terms of OH exposure, in addition to reaction time.

2.2 Computational methods

2.2.1 Mie theory calculations

To verify that changes in SSA during heterogeneous OH oxidation were induced by chemical changes to the aerosol, rather than small changes in the size distributions, we compared the observed trends to modelled trends, based on the observed size distributions and an assumed, constant complex refractive index, $m = n + ik$, where n and k are the real and imaginary parts, respectively. Lognormal curves were fit to the raw geometric-cross-section-weighted size distributions (see Fig. 2a), and the absorption and scattering efficiencies for 405 nm light of individual channels between about 20 and 600 nm were calculated from the complex refractive index of the initial BrC particles, which are assumed to be spherical and homogeneously mixed, using the program Mie3Layer (Charamisinau et al., 2005). The absorption and scattering coefficients were calculated for each channel, and total values across the distribution were used to calculate the SSA of the whole aerosol population.

2.2.2 Multi-layer kinetics modelling

To better understand the effects of RH on the evolution of the optical properties of the BrC surrogate, we constructed a multi-layer kinetics model based on the Pöschl-Rudich-Ammann (PRA) framework (Ammann and Pöschl, 2007; Pöschl et al., 2007). The model particles consist of a surface layer, two near-surface bulk layers, and the remaining bulk phase, as illustrated in Fig. 3. The near-surface bulk layers are included to account for concentration gradients in the bulk phase (Shiraiwa et al., 2010); each is 2 nm thick. The diameter and density of the particles are assumed to be 180 nm and 1.3 g cm^{-3}, respectively. The particles are assumed to be initially composed of a single BrC species, A. At the surface, A reacts with OH to form product B, and B reacts to form product C. The loss of species i = A, B due to reaction with OH, L_i, is calculated as $\gamma_{\mathrm{OH},i} J_{\mathrm{OH}} \theta_i$, where $\gamma_{\mathrm{OH},i}$ is the probability that a collision between OH and species i leads to reaction, J_{OH} is the flux of OH to the particles per unit of surface area, and θ_i is the fractional surface coverage of species i (Shiraiwa et al., 2009). ~~To limit the degrees of freedom, we assume that $\gamma_{\mathrm{OH},i}$ is the same for A and B.~~

The rate constant for diffusion between bulk layers, $k_{\mathrm{b,b},i}$, is calculated as $4D_{\mathrm{b},i}/(\pi\delta)$, where $D_{\mathrm{b},i}$ is the bulk diffusion coefficient of species i, and δ is the layer thickness (Shiraiwa et al., 2010). For the transfer from the near-surface bulk layer 1 to the surface, $k_{\mathrm{b1,s},i}$, δ above is substituted with $(\delta+\delta_{\mathrm{A}})/2$, where δ_{A} is the effective molecular diameter of A (Shiraiwa et al., 2010). Though B may form from oligomerization of compounds grouped into species A, we assume that the effective molecular diameters of all species are the same. We also assume the species have the same bulk diffusion coefficients, ensuring that the total concentration in the surface layer is the same as the number of surface sites. The rate constant for diffusion from the surface to the near-surface bulk layer 1, $k_{\mathrm{s,b1},i}$, is taken as $k_{\mathrm{b1,s},i}/\delta_{\mathrm{A}}$.

The above considerations allow us to calculate concentrations of A, B, and C in the surface and bulk layers. However, to compare the modelled and experimental results, we must calculate the relative absorption of the model particles. We derive the relative absorption of the particles solely from the concentrations and molar absorptivities, as in a bulk solution; i.e., the absorption that would be measured upon particle-into-liquid sampling. This modelled relative absorption is compared to the experimental absorption coefficient normalized to that which would be expected if the initial complex refractive index (*m*) did not change during the experiment, accounting for size dependence. Experimental times series of this normalized absorption were derived for photolysis and heterogeneous OH oxidation experiments, and the latter were corrected for the effect of photolysis. ~~During heterogeneous OH oxidation, the evolution of the SSA of the particles incorporates changes in both absorption and scattering. However, the changes in absorption are likely dominant. For example, for fixed values of *n* (1.35) and particle diameter (200 nm), a 50% decrease in *k* (from 0.04 to 0.02) gives a 10% increase in Q_{sca} but almost a 50% decrease in Q_{abs}. Consequently, we assume that Q_{sca} is steady, and we compare the modelled trends in relative absorption to the experimental trends in the inverse of relative SSA.~~

Processes other than directly OH-initiated oxidation also occur. For example, radical products of the initial OH reaction likely form RO_2 species by reaction with O_2. These RO_2 species may react with each other in a termination step or react with NO, for example, to form RO (Richards-Henderson et al., 2015, 2016), which may initiate further oxidation of the brown carbon constituents. They may also facilitate auto-oxidation by abstracting hydrogen from adjacent groups on the same or neighbouring molecules. We do not consider these processes in our simple multi-phase kinetics model, since many other parameters, such as the diffusion coefficient of O_2 in the particles and the absorptivities of any additional products, would have to be introduced, but they may play a role in the apparent values of uptake coefficients.

3 Results and discussion

3.1 Initial BrC surrogate

To produce a laboratory surrogate of secondary BrC, we generated a mixture of light-absorbing products by the aqueous photo-oxidation of resorcinol and H_2O_2 exposed to UV-B radiation. Initially, the solution of resorcinol and H_2O_2 exhibited no absorption of light at visible wavelengths, as shown in Fig. S2. Following 4 h of photo-oxidation, the solution was highly coloured, exhibiting broad absorption features that were strongly dependent on wavelength, such that absorbance across a 1-cm pathlength was about 0.6 at 400 nm but negligible at >600 nm (see Fig. S2). In the past, light-absorbing products of the aqueous photo-oxidation of resorcinol were also observed by Chang and Thompson (2010), who used 1 mM H_2O_2. Here, the concentration of H_2O_2 was an order of magnitude greater, and the colour developed slightly faster, as illustrated by the time series of absorbance at 450 nm (see Fig. S3).

More generally, light-absorbing products of aqueous photo-oxidation have been observed for a wide range of phenolic species, including those with methyl, methoxy, and carbonyl substituents (Chang and Thompson, 2010; Gelencsér et al., 2003; Smith et al., 2016). In detailed mechanistic studies, products of both hydroxylation and oligomerization have been identified (Hoffer et al., 2004; Li et al., 2014; Sun et al., 2010; Yu et al., 2014, 2016). Oligomers form by C–C or C–O radical coupling (Kobayashi and Higashimura, 2003). C–C coupling might be expected to lead to greater absorption enhancement, since the resulting biphenyls and larger oligomers may have some degree of delocalization across the rings (Zhang et al., 2010). Indeed, based on density functional theory calculations, Magalhães et al. (2017) have shown that the absorptivity of bi- and terphenyls is greater in water than in the gas phase, because the planarity and delocalization increase. Interestingly, five of the ten most abundant products of the aqueous photo-oxidation of 0.1 mM syringol with 0.1 mM H_2O_2 have been shown to be biphenyls (Yu et al., 2014). The concentration of the phenolic precursor used here was two orders of magnitude greater, a condition that may favour oligomerization over hydroxylation. Fragmentation may also occur during aqueous photo-oxidation, but the volatile products are removed in the activated carbon denuders, following atomization. Based on these considerations, the secondary BrC aerosol is likely composed primarily of oligomers, and we assume the average molecular mass is 326 g mol^{-1}, representative of a terphenyl product of resorcinol.

Before investigating the effects of photolysis and heterogeneous OH oxidation on the optical properties of the BrC surrogate, we performed control experiments, without either H_2O_2 or irradiation, to constrain the size-dependence of the optical properties. Results from a deposition experiment at 60% RH, in which BrC was injected into the chamber and diluted with clean humidified air, are shown in Fig. 4. The initial geometric mean number diameter and standard deviation were 125 nm and 1.5, respectively, and the initial SSA was about 0.76. When the particles were unperturbed by radiation or OH, they were simply lost by dilution and deposition. Because smaller particles deposit faster than larger ones, the geometric mean surface diameter gradually increased from about 170 to 190 nm over the course of 3 h. Both the absorption and scattering coefficients steadily decreased as particles were continuously lost, but the SSA increased slightly (see Fig. 2b) due to the increase in geometric mean surface diameter.

This observed size dependence of SSA can be compared to Mie theory calculations, based on the measured size distributions and an assumed complex refractive index. The complex refractive index should not change without photolysis or heterogeneous OH oxidation, so we manually scanned values of *n* and *k* to apply for the duration of the experiment. We found that *n* and *k* values of 1.35 and 0.046, respectively, are suitable to reproduce the evolution of SSA in this particular experiment (see Fig. 4b). Stepping *n* from 1.40 to 1.55 and adjusting *k* accordingly demonstrates that the good agreement for this refractive index is unique, as shown in Fig. S4. We stress that even an approximate value of the refractive index is adequate to distinguish whether changes in the SSA are due to changes in the size distribution or chemical composition. For SOA generated from anthropogenic and biogenic volatile organic compounds, *n* values ranging from 1.35 to 1.61 have been observed (Kim and Paulson, 2013). The value of *k* is in the regime of previous observations for BrC at 405 nm, which vary from very low values of 0.004 (Cappa et al., 2012) and 0.007 (Lack et al., 2012) to 0.112 (at 400 nm) (Kirchstetter et al., 2004). In a recent field study in India, a similar value of 0.037 for ambient BrC was observed (Shamjad et al., 2016).

In one experiment, BrC particles were sampled from the chamber alternately with and without a diffusion dryer upstream of the DMA. The conditioning was alternated every 15 min, allowing time for the RH of the sheath flow to stabilize. As shown in Fig. S5, the size distribution slowly shifts to larger mobility diameters, because smaller particles are lost faster than larger particles. Besides this trend, the variation between the conditions is negligible, so there is not significant water uptake at 60% RH.

3.2 Evolution of BrC due to photolysis

Having constrained the size-dependence of the optical properties, based on the closure between measured and calculated SSA values, we now consider the effects of photolysis on the optical properties of the BrC surrogate. The emission of the UV-B black-lights ~~–~~in the chamber, with a peak at 310 nm, ~~–~~is not representative of natural sunlight, so we do not draw direct comparisons between the timescale of our experiments and that of photolysis in the atmosphere. Rather, we performed photolysis experiments to account for the effects of photolysis during the heterogeneous OH oxidation experiments. Wong et al. (2015) have shown that for this chamber equipped with UV-B bulbs, the photo flux at wavelengths below 310 nm is much greater than for a clear-sky summer day; for example, at 300 nm, the photon flux from the bulbs is close to its peak value of about 1 x 10^{14} photons s^{-1} cm^{-2} nm^{-1}, while the photon flux outside is negligible. Light at wavelengths below 310 nm is likely driving most of the photo-chemistry during the photolysis experiments, so we believe the relative impact of photolysis would be small in the atmosphere, even considering that the ambient OH concentration is lower than in the chamber.

Results from a photolysis experiment at 60% RH are illustrated in Fig. 5. In each experiment, the value of *n* was taken as 1.35, as described above; the assumption that *n* is constant for the duration of the experiment is supported by the previous observation that, for BrC generated from ammonium sulfate and methylglyoxal, *n* did not change as the reaction proceeded (Tang et al., 2016). Despite closely reproducing the preparation of the BrC surrogate solution and injecting to approximately the same total particle volume in each experiment, we observed small differences in initial size distributions and SSA values, so it was necessary to vary *k* slightly from experiment to experiment. For the calculated SSA to follow the trend observed before the lights are turned on, at relative time zero, a *k* value of 0.040 must be adopted. When strict comparisons are made between experiments, the relative SSA (the current SSA divided by the initial SSA) is presented. In 3 h, the geometric mean surface diameter increased from about 160 to 180 nm, similar to the deposition experiment, so little or no volatilization of the particles can be inferred. Because the diameter increased uniformly, the predicted SSA increases steadily. In contrast, the observed SSA gradually decreased once the lights were turned on, indicating that the particles slowly became more absorbing.

Photolysis has been observed to lead to absorption enhancement of other BrC surrogates in the past (Saleh et al., 2013; Wong et al., 2017; Zhao et al., 2015; Zhong and Jang, 2014). For example, the absorbance at 400 nm of water-soluble species produced by combustion of kaoliang stalk has been shown to increase during the first 30 min of irradiation in a solar simulator (Zhao et al., 2015). Recently, the peak absorption enhancement due to photolysis of biomass burning BrC constituents has been shown to increase with their molecular mass (Wong et al., 2017). Since the trace gas denuders remove volatile species after atomization, the composition of the particles is likely skewed towards an average molecular mass that is larger than that of the species in solution, possibly making the particles more susceptible to photolysis. In general, absorption enhancement may occur due to direct photolysis of chromophores, followed by radical recombination leading to larger, more absorptive oligomers, or reactions with OH from the dissociation of H_2O_2 generated from the photolysis of carbonyl compounds in the condensed phase (Anastasio et al., 1997; von Sonntag and Schuchmann, 1991). In the past, the absorption enhancement of biomass burning BrC exposed to natural sunlight has been shown to increase with RH (Zhong and Jang, 2014), a trend that was attributed to the increasing production and dissociation of H_2O_2 with increasing RH. Here, we observe similar trends in relative SSA under both low and high RH conditions (see Fig. 6b). It is unlikely that sufficient OH could be produced in the particle phase at the lower RH, so indirect photolysis of carbonyl compounds likely does not have a significant role in the observed absorption enhancement.

In past studies, the period of absorption enhancement due to photolysis has been shown to be followed by bleaching (Wong et al., 2017; Zhao et al., 2015; Zhong and Jang, 2014). In the present experiments, the irradiation time is limited by the particle losses; after about 3 h, the scattering and absorption coefficients approach the detection limits of the PASS. Near the end of the photolysis experiments, SSA levelled off, and this period may coincide with the inflection point between absorption enhancement and bleaching.

3.3 Evolution of BrC due to heterogeneous OH oxidation

The evolution of the optical properties of the BrC surrogate during a photo-oxidation experiment is affected by deposition, photolysis, and heterogeneous OH oxidation. Results of a representative photo-oxidation experiment at 60% RH are shown in Fig. 7; replicate experiments were performed at each RH. The initial geometric mean surface diameter was slightly higher than in the photolysis experiment described above (about 196 nm compared to 160 nm), so although the initial aerosol was slightly more scattering (higher SSA), the value of *k* required to reproduce the SSA before irradiation is ~~slightly higher~~very similar (0.041 compared to 0.040). During irradiation, the geometric mean surface diameter first increased slightly due to deposition and then began to decrease due to volatilization. As a result, the predicted SSA first increases slightly and then, at about 90 min, begins to decrease. The observed SSA exhibited a sharp decrease within only 10 min of reaction time and an induction period before a significant increase. Both the absorption enhancement and bleaching contrast with the predicted trend of SSA, so they are certainly due to the evolution of particle composition, rather than size. The absorption enhancement was rapid enough to lead to a peak in the absorption coefficient, despite continuous particle losses (see Fig. S64).

As described above, evaporation of water from particles can result in a negative bias in photo-acoustic measurements (Langridge et al., 2013). If heterogeneous OH oxidation significantly increased the hygroscopicity of the particles, the water content of the aerosol would increase during the experiment. The resulting increase in the magnitude of the bias could contribute to apparent bleaching. In addition to this instrumental artifact, progressively more water uptake could lead to genuinely greater scattering coefficients, which would also result in apparent bleaching. We investigated these potential effects by alternately sampling with and without a diffusion dryer downstream of the chamber at 60% RH. As shown in Fig. S7, the absorption coefficient does not depend on the conditioning. The scattering coefficient is about 10% lower for the dried particles (see Fig. S8), but this difference is roughly steady during photo-oxidation. In other words, the particles do not become significantly more hygroscopic, and the changes in absorption and scattering coefficients are indeed due to the chemical evolution of the particles.

To ensure that the sequential absorption enhancement and bleaching described above are distinctive features of the BrC surrogate, we also investigated the heterogeneous OH oxidation of a yellow dye aerosol at 60% RH. In this case, we observed uniform bleaching, as shown in Fig. ~~S5~~S9, consistent with bulk aqueous studies of similar azo dyes (Georgiou et al., 2002). There was no decrease in the geometric mean surface diameter, so there was little or no volatilization. It is likely that OH attacks the azo nitrogen-nitrogen bond (Hisaindee et al., 2013). The product fragments would be large enough to remain in the particle phase; for example, the smaller fragment would still contain one sulfonate group and two aromatic rings.

Unlike photolysis, heterogeneous OH oxidation is strongly dependent on RH, as shown in Fig. 6a. In contrast to the rapid absorption enhancement and bleaching observed at 60% RH, the period of absorption enhancement is prolonged at 15% RH, on a timescale similar to that of the photolysis experiments. The peak absorption enhancement at 15% RH results in a lower relative SSA than at 60% RH. To better understand the effects of RH on heterogeneous OH oxidation, we compare experimental results with those of the multi-layer kinetics model described above. In all, the model has ~~four~~ five adjustable parameters: ~~the~~ two uptake coefficients, $\gamma_{\mathrm{OH},i}$; the diffusion coefficient, $D_{\mathrm{b},i}$; and the molar absorptivities of products B and C, ε_{B}, and ε_{C}, respectively.

At 60% RH, the experimental features can be reproduced (see Fig. 8) by setting $\gamma_{\mathrm{OH},\cancel{i}\mathrm{A}}$ and $\gamma_{\mathrm{OH,B}}$ to ~~4.2~~5.0 and 7.5, respectively, suggesting that oxidation is very efficient. An uptake coefficient, $\gamma_{\mathrm{OH,A}}$, greater than unity indicates that each collision between OH and A leads to the formation of more than one molecule of B. In previous heterogeneous OH oxidation experiments, a wide range of OH uptake coefficients have been observed, including values greater than unity (George and Abbatt, 2010). In the particle phase, oxidation initiated by OH may form products directly from reactions with OH or indirectly from organic radicals, RO. The organic radicals may result from free radical chain reactions that have been shown to lead to very high effective uptake coefficients, in particular, when species like NO and SO_2 are present to enhance conversion of RO_2 to RO (Richards-Henderson et al., 2015, 2016). We note that the values of $\gamma_{\mathrm{OH},i}$ ~~is~~ are dependent on the assumed average molecular mass, which is set to 326 g mol^{-1}, representative of a terphenyl oligomerization product of resorcinol, as discussed above. A greater molecular mass would result in ~~a~~ lower values of $\gamma_{\mathrm{OH},i}$, so we cannot be sure to what extent~~whether~~ free radical chain reactions are playing a role in the experiments. Scaling the uptake coefficients such that $\gamma_{\mathrm{OH,A}}$ decreases from 5.0 to 1.0 requires increasing the molecular weight from 326 to 1600 g mol^{-1}. It is difficult to rationalize such large oligomers forming during the 4-h aqueous photo-oxidation, so secondary radicals are indeed likely contributing to oxidation. Furthermore, we assume that OH undergoes solely gas-surface reactions, following Shiraiwa et al. (2009). Recent measurements indicate that this may be an over-simplification, as the reactive-diffusive length of OH in squalene is similar to that of ozone (Lee and Wilson, 2016), so surface-layer reactions may also occur. Nonetheless, we can state with confidence that the oxidation is very efficient.

We find that the observed trend in relative absorption at 60% RH – in particular, the significant bleaching – can~~not~~ be reproduced only if the aging particles are taken as well-mixed, so diffusion of A from the bulk to the surface is not restricted~~;~~ ~~if $D_{\mathrm{b},i}$ is taken as 1 x 10^{-14} cm^2 s^{-1}, the decay in the concentration of A is about the same in all three bulk layers (see Fig. S6a), and the abrupt cessation of absorption enhancement cannot be captured. As shown in Fig. S7, if the absorptivities are fixed, and the uptake coefficient is scanned from 0.2 to 10, the trends in relative absorption have the same shape (simply stretched or compressed along the time axis), because the particles are well-mixed. On the other hand, if $D_{\mathrm{b},i}$ is taken as 1 x 10^{-16} cm^2 s^{-1}, the fraction of species A at the surface decays faster than in the bulk (see Fig. S6c), the modelled trends cannot be superimposed by scaling along the time axis (see Fig. S8), and the abrupt cessation of absorption enhancement to be captured.~~ As shown in Fig. 8b, the concentrations of A, B, and C are the same in all four layers. At 60% RH, secondary organic material derived from the gas-phase photo-oxidation of toluene has a diffusion coefficient on the order of 10^{-10} cm^2 s^{-1} (Song et al., 2016). Here, any value greater than 1 x 10^{-14} cm^2 s^{-1} gives good agreement, so $D_{\mathrm{b},i}$ is set to 1 x 10^{-14} cm^2 s^{-1} as a lower limit. ~~Though the present diffusion coefficient is surprisingly low, it is possible that the secondary organic material formed from resorcinol in the aqueous phase is primarily oligomeric and comparatively viscous even at 60% RH.~~ Though the extent of bleaching is captured by the model, rapid initial colour enhancement is not. We speculate the other processes, like auto-oxidation, could contribute to this feature. The same diffusion coefficient is assumed for all three species, but in reality $D_{\mathrm{b},i}$ may increase in going from A to B and decrease in going from B to C; if C is a product of fragmentation, it might be expected to have a greater diffusion coefficient in A than the self-diffusion coefficient of A. Indeed, plasticization has been shown to occur during heterogeneous OH oxidation of semi-solid alkane particles at high gas-phase OH concentrations (Wiegel et al., 2017).

Finally, the experimental features are reproduced by setting the molar absorptivities of B and C (ε_{B} and ε_{C}) to ~~2~~1.5ε_{A} and ~~0~~zero, respectively. We note that this combination of parameters is likely one of several possible solutions. Even for a more tightly-constrained set of experimental data regarding consumption of oleic acid by heterogeneous reactions with ozone (Ziemann, 2005), more than one model scenario has been found to adequately reproduce observations of the number of oleic acid molecules in the particle phase (Pfrang et al., 2010).

At 15% RH, the experimental features are reproduced (see Fig. 8) by setting $\gamma_{\mathrm{OH,A}}$ and $\gamma_{\mathrm{OH,B}}$~~$\gamma_{\mathrm{OH},i}$~~ to 1.0 and 0.1, respectively, and $D_{\mathrm{b},i}$ to ~~1.0 and~~ 1 x 10~~$^{-18}$~~$^{-16}$ cm^2 s^{-1}~~, respectively~~. The decreases in the uptake coefficients with RH ~~in $\gamma_{\mathrm{OH},i}$~~

~~from 4.2 to 1.0~~ may be the result of differences in the distribution of initial BrC species in the particle or the orientation of the species at the surface. The decrease in $D_{\mathrm{b},i}$ by two orders of magnitude is reasonable, considering the significant RH-dependence of viscosity observed for secondary organic material derived from toluene and isoprene (Song et al., 2015, 2016). ~~An upper limit to t~~The diffusion coefficient of secondary organic material derived from toluene was found to be less than ~~about~~ 10^{-17} cm^2 s^{-1} ~~was found~~ for RH ≤ 17% (Song et al., 2016). ~~Based on the absence of bleaching during the experimental timescale~~ As before, we set ε_B and ε_C to 1.5ε_A and zero. ~~ε_C to be the same as ε_B; i.e., 2.5ε_A (see Fig. S9). This equivalence may indicate that, if fragmentation occurs due to reaction of OH with B, the strict confinement of the fragments leads to recombination, such that the absorption persists.~~ It is ~~also~~ possible that ~~stable~~ fragmentation products ~~form, but they~~ volatilize out of the condensed phase to a ~~much~~ greater extent than they diffuse to the bulk phase, because the particles are so viscous~~; in this case, the decreased molar absorptivity of the products would have little effect on the total particle absorption~~. In fact, a slight decrease in the mean geometric surface diameter suggests that there is some degree of volatilization. On a related note, because the viscosity is so high, the products B and C are much more concentrated at the surface than in the bulk layers (see Fig. ~~9~~8c). Consequently, at 15% RH, the ~~aged~~ aging particles likely consist of less absorbing cores and highly absorbing shells~~consist of unchanged BrC cores encased in thin, more-absorptive shells~~.

In general, we emphasize that the set of molecular properties presented above, which best fit the experimental data, were selected after multiple trials with different input parameter values and different model scenarios, as well. Although the mechanism and final parameter set fit the data remarkably well, we acknowledge that the complex nature of the inherent chemistry, with changes in optical properties occurring alongside concentration, suggest that this parameter set should only be viewed semi-quantitatively; i.e., the solution is most useful for substantiating the mechanism leading to the changes in absorption.

4 Conclusions and atmospheric implications

In this study, we have demonstrated for the first time that secondary BrC aerosol derived from a phenolic precursor is susceptible to further photo-chemical aging after cloud processing and droplet evaporation. Specifically, at 60% RH, OH exposure induced rapid absorption enhancement followed by relatively slow bleaching of the surrogate BrC aerosol; at 15% RH, OH exposure induced only slow absorption enhancement. Moreover, we have constructed a multi-layer kinetics model that captures the general features of the evolution of the optical properties of the particles. The candidate parameters suggest that the oxidation is very efficient, possibly even involving free radical chain reactions, and the surrogate BrC aerosol is very viscous. Free radical chain reactions may be more important in the atmosphere, where a lower concentration of OH results in a lower concentration of RO_2 and a reduced probability of chain termination reactions. Furthermore, the presence of other pollutants like NO may enhance the conversion of RO_2 to RO (Richards-Henderson et al., 2015). Since the BrC is very viscous, it is important that the experimental timescale approximates the atmospheric timescale, so species are allowed sufficient time to diffuse within the particles. In the laboratory, flow-tube experiments with higher OH concentrations and shorter timescales than photo-oxidation chamber experiments may not as accurately account for free radical chain reactions and diffusion timescales.

Using our measurements and those of others, we can now speculate on the photochemical behaviour of BrC in the atmosphere. Recently, Sumlin et al. (2017) observed bleaching due to heterogeneous OH oxidation of primary BrC derived from ~~biomass~~ burning of a number of types of biomass fuels, which lost almost 50% of its absorption at 375 and 405 nm after the equivalent of about 4.5 days in the atmosphere. In our experiments at 60% RH, the SSA of the BrC first increased and then decreased to its initial value after about 2 h of photo-oxidation in the chamber; in the atmosphere, this would correspond to about 30 h, because the average OH concentration in the chamber (1.6 x 10^7 molecule cm^{-3}) is considerably greater than typical OH concentrations in the atmosphere (on the order of 10^6 molecule cm^{-3}). In other words, the initial, rapid absorption enhancement could compensate for more than a day of bleaching. In the atmosphere, then, we may expect highly variable evolution of biomass burning plumes. If little or no secondary BrC forms, bleaching of primary BrC will dominate, and the absorption will decay uniformly. Indeed, Forrister et al. (2015) have observed such a trend in the field. If considerable secondary BrC forms, e.g., by cloud processing, some additional absorption will develop. We have shown that additional absorption may develop after cloud processing, as well. These processes will compete with the bleaching of primary BrC, such that the total BrC absorption may persist for longer periods. Indeed, Zhang et al. (2017) observed that the absorption by BrC at 365 nm was largely preserved during convection and one day of residence in the upper troposphere. Our results suggest that the persistence of BrC in this field study was the result of absorption enhancement compensating for bleaching, rather than recalcitrance of the BrC. We speculate that, upon further aging of this plume, bleaching would begin to play a greater role than absorption enhancement. In the 15% RH experiment, only absorption enhancement was observed after the equivalent of about 40 h in the atmosphere. Though such low RH conditions are less widely applicable in the atmosphere, there may be scenarios in which bleaching due to heterogeneous OH oxidation does not occur even days after secondary BrC formation from cloud processing of phenolic species.

The aerosol studied here is a reasonable proxy for the secondary BrC that may form in the atmosphere upon evaporation of cloud droplets. Biomass burning emits BC, primary BrC, and non-absorbing organic compounds, in both the gas and particle phases. These organic compounds include phenolic species, derived from the decomposition of lignin during combustion (Simoneit, 2002). Resorcinol is a representative phenolic emission of biomass burning (Simoneit, 2002; Veres et al., 2010; Wang et al., 2009); for example, Schauer et al. (2001) observed about 50 μg of resorcinol from the combustion of 1 kg of wood. Furthermore, about 95% of the resorcinol was in the particle phase, compared to about 55 and 0% for the 1,4- and 1,2-dihydroxybenzene isomers, respectively. Whether in the aerosol phase or in cloud droplets, resorcinol and other phenolic species may react with OH to form chromophores, like the bi- and terphenyl products discussed above. Interestingly, biphenyls have recently been identified in ambient cloud water (Cook et al., 2017). The formation of secondary BrC from OH oxidation of phenolic species during the day contrasts with some other routes of secondary BrC formation that occur at night and result in chromophores – e.g., pyruvic acid polymers (Rincón et al., 2009) and imine compounds (Zhao et al., 2015) – that may be bleached comparatively quickly. The photochemical behaviour of these and other classes of secondary BrC chromophores plays an important role in the overall climate effects of BrC, and similar experiments should be performed for other surrogates in the future.

Acknowledgements. This research was funded by the Natural Sciences and Engineering Research Council of Canada (NSERC). E. G. Schnitzler gratefully acknowledges a Postdoctoral Fellowship from NSERC.

References

Abu-Rahmah, A., Arnott, W. P. and Moosmüller, H.: Integrating nephelometer with a low truncation angle and an extended calibration scheme, Meas. Sci. Technol., 17, 1723, doi:10.1088/0957-0233/17/7/010, 2006.

Alexander, D. T. L., Crozier, P. A. and Anderson, J. R.: Brown carbon spheres in East Asian outflow and their optical properties, Science, 321, 833–836, doi:10.1126/science.1155296, 2008.

Ammann, M. and Pöschl, U.: Kinetic model framework for aerosol and cloud surface chemistry and gas-particle interactions – Part 2: Exemplary practical applications and numerical simulations, Atmos. Chem. Phys., 7, 6025–6045, doi:10.5194/acp-7-6025-2007, 2007.

Anastasio, C., Faust, B. C. and Rao, C. J.: Aromatic carbonyl compounds as aqueous-phase photochemical sources of hydrogen peroxide in acidic sulfate aerosols, fogs, and clouds. 1. Non-Phenolic methoxybenzaldehydes and methoxyacetophenones with reductants (phenols), Environ. Sci. Technol., 31, 218–232, doi:10.1021/es960359g, 1997.

Atkinson, R. and Arey, J.: Atmospheric degradation of volatile organic compounds, Chem. Rev., 103, 4605–4638, doi:10.1021/cr0206420, 2003.

Bahadur, R., Praveen, P. S., Xu, Y. and Ramanathan, V.: Solar absorption by elemental and brown carbon determined from spectral observations, Proc. Natl. Acad. Sci., 109, 17366–17371, doi:10.1073/pnas.1205910109, 2012.

Baker, M. B.: Energy absorption by volatile atmospheric aerosol particles, Atmos. Environ. 1967, 10, 241–248, doi:10.1016/0004-6981(76)90097-4, 1976.

Bluvshtein, N., Flores, J. M., He, Q., Segre, E., Segev, L., Hong, N., Donohue, A., Hilfiker, J. N. and Rudich, Y.: Calibration of a multi-pass photoacoustic spectrometer cell using light-absorbing aerosols, Atmos. Meas. Tech., 10, 1203–1213, doi:10.5194/amt-10-1203-2017, 2017.

Bond, T. C.: Spectral dependence of visible light absorption by carbonaceous particles emitted from coal combustion, Geophys. Res. Lett., 28, 4075–4078, doi:10.1029/2001GL013652, 2001.

Cappa, C. D., Onasch, T. B., Massoli, P., Worsnop, D. R., Bates, T. S., Cross, E. S., Davidovits, P., Hakala, J., Hayden, K. L., Jobson, B. T., Kolesar, K. R., Lack, D. A., Lerner, B. M., Li, S.-M., Mellon, D., Nuaaman, I., Olfert, J. S., Petäjä, T., Quinn, P. K., Song, C., Subramanian, R., Williams, E. J. and Zaveri, R. A.: Radiative absorption enhancements due to the mixing state of atmospheric black carbon, Science, 337, 1078–1081, doi:10.1126/science.1223447, 2012.

Chakrabarty, R. K., Moosmüller, H., Chen, L.-W. A., Lewis, K., Arnott, W. P., Mazzoleni, C., Dubey, M. K., Wold, C. E., Hao, W. M. and Kreidenweis, S. M.: Brown carbon in tar balls from smoldering biomass combustion, Atmos. Chem. Phys., 10, 6363–6370, doi:10.5194/acp-10-6363-2010, 2010.

Chang, J. L. and Thompson, J. E.: Characterization of colored products formed during irradiation of aqueous solutions containing H_2O_2 and phenolic compounds, Atmos. Environ., 44, 541–551, doi:10.1016/j.atmosenv.2009.10.042, 2010.

Charamisinau, I., Happawana, G., Evans, G., Rosen, A., His, R. A. and Bour, D.: Semiconductor laser insert with uniform illumination for use in photodynamic therapy, Appl. Opt., 44, 5055–5068, doi:10.1364/AO.44.005055, 2005.

Chen, Y. and Bond, T. C.: Light absorption by organic carbon from wood combustion, Atmos. Chem. Phys., 10, 1773–1787, doi:10.5194/acp-10-1773-2010, 2010.

Chung, C. E., Ramanathan, V. and Decremer, D.: Observationally constrained estimates of carbonaceous aerosol radiative forcing, Proc. Natl. Acad. Sci., 109, 11624–11629, doi:10.1073/pnas.1203707109, 2012.

Cook, R. D., Lin, Y.-H., Peng, Z., Boone, E., Chu, R. K., Dukett, J. E., Gunsch, M. J., Zhang, W., Tolic, N., Laskin, A., and Pratt, K. A.: Biogenic, urban, and wildfire influences on the molecular composition of dissolved organic compounds in cloud water, Atmos. Chem. Phys., 17, 151567–15180, doi:10.5194/acp-2017-628, 2017.

De Haan, D. O., Tolbert, M. A. and Jimenez, J. L.: Atmospheric condensed-phase reactions of glyoxal with methylamine, Geophys. Res. Lett., 36, L11819, doi:10.1029/2009GL037441, 2009.

De Haan, D. O., Hawkins, L. N., Kononenko, J. A., Turley, J. J., Corrigan, A. L., Tolbert, M. A. and Jimenez, J. L.: Formation of nitrogen-containing oligomers by methylglyoxal and amines in simulated evaporating cloud droplets, Environ. Sci. Technol., 45, 984–991, doi:10.1021/es102933x, 2011.

Del Vecchio, R. and Blough, N. V.: On the origin of the optical properties of humic substances, Environ. Sci. Technol., 38, 3885–3891, doi:10.1021/es049912h, 2004.

Di Lorenzo, R. A. and Young, C. J.: Size separation method for absorption characterization in brown carbon: Application to an aged biomass burning sample, Geophys. Res. Lett., 43, 2015GL066954, doi:10.1002/2015GL066954, 2016.

Di Lorenzo, R. A., Washenfelder, R. A., Attwood, A. R., Guo, H., Xu, L., Ng, N. L., Weber, R. J., Baumann, K., Edgerton, E. and Young, C. J.: Molecular-size-separated brown carbon absorption for biomass-burning aerosol at multiple field sites, Environ. Sci. Technol., 51, 3128–3137, doi:10.1021/acs.est.6b06160, 2017.

Forrister, H., Liu, J., Scheuer, E., Dibb, J., Ziemba, L., Thornhill, K. L., Anderson, B., Diskin, G., Perring, A. E., Schwarz, J. P., Campuzano-Jost, P., Day, D. A., Palm, B. B., Jimenez, J. L., Nenes, A. and Weber, R. J.: Evolution of brown carbon in wildfire plumes, Geophys. Res. Lett., 42, 2015GL063897, doi:10.1002/2015GL063897, 2015.

Gelencsér, A., Hoffer, A., Kiss, G., Tombácz, E., Kurdi, R. and Bencze, L.: In-situ formation of light-absorbing organic matter in cloud water, J. Atmos. Chem., 45, 25–33, doi:10.1023/A:1024060428172, 2003.

George, I. J. and Abbatt, J. P. D.: Heterogeneous oxidation of atmospheric aerosol particles by gas-phase radicals, Nat. Chem., 2, 713–722, doi:10.1038/nchem.806, 2010.

~~George, I. J., Vlasenko, A., Slowik, J. G., Broekhuizen, K. and Abbatt, J. P. D.: Heterogeneous oxidation of saturated organic aerosols by hydroxyl radicals: uptake kinetics, condensed-phase products, and particle size change, Atmos. Chem. Phys., 7, 4187–4201, doi:10.5194/acp-7-4187-2007, 2007.~~

Georgiou, D., Melidis, P., Aivasidis, A. and Gimouhopoulos, K.: Degradation of azo-reactive dyes by ultraviolet radiation in the presence of hydrogen peroxide, Dyes Pigments, 52, 69–78, doi:10.1016/S0143-7208(01)00078-X, 2002.

Gilardoni, S., Massoli, P., Paglione, M., Giulianelli, L., Carbone, C., Rinaldi, M., Decesari, S., Sandrini, S., Costabile, F., Gobbi, G. P., Pietrogrande, M. C., Visentin, M., Scotto, F., Fuzzi, S. and Facchini, M. C.: Direct observation of aqueous secondary organic aerosol from biomass-burning emissions, Proc. Natl. Acad. Sci., 113, 10013–10018, doi:10.1073/pnas.1602212113, 2016.

Hisaindee, S., Meetani, M. A. and Rauf, M. A.: Application of LC-MS to the analysis of advanced oxidation process (AOP) degradation of dye products and reaction mechanisms, TrAC Trends Anal. Chem., 49, 31–44, doi:10.1016/j.trac.2013.03.011, 2013.

Hoffer, A., Kiss, G., Blazsó, M. and Gelencsér, A.: Chemical characterization of humic-like substances (HULIS) formed from a lignin-type precursor in model cloud water, Geophys. Res. Lett., 31, L06115, doi:10.1029/2003GL018962, 2004.

Hoffer, A., Tóth, A., Nyirő-Kósa, I., Pósfai, M. and Gelencsér, A.: Light absorption properties of laboratory-generated tar ball particles, Atmos. Chem. Phys., 16, 239–246, doi:10.5194/acp-16-239-2016, 2016.

Kim, H. and Paulson, S. E.: Real refractive indices and volatility of secondary organic aerosol generated from photooxidation and ozonolysis of limonene, α-pinene and toluene, Atmos. Chem. Phys., 13, 7711–7723, doi:10.5194/acp-13-7711-2013, 2013.

Kirchstetter, T. W., Novakov, T. and Hobbs, P. V.: Evidence that the spectral dependence of light absorption by aerosols is affected by organic carbon, J. Geophys. Res. Atmos., 109, D21208, doi:10.1029/2004JD004999, 2004.

Kobayashi, S. and Higashimura, H.: Oxidative polymerization of phenols revisited, Prog. Polym. Sci., 28, 1015–1048, doi:10.1016/S0079-6700(03)00014-5, 2003.

Lack, D. A., Lovejoy, E. R., Baynard, T., Pettersson, A. and Ravishankara, A. R.: Aerosol absorption measurement using photoacoustic spectroscopy: Sensitivity, calibration, and uncertainty developments, Aerosol Sci. Technol., 40, 697–708, doi:10.1080/02786820600803917, 2006.

Lack, D. A., Langridge, J. M., Bahreini, R., Cappa, C. D., Middlebrook, A. M. and Schwarz, J. P.: Brown carbon and internal mixing in biomass burning particles, Proc. Natl. Acad. Sci., 109, 14802–14807, doi:10.1073/pnas.1206575109, 2012.

Lambe, A. T., Cappa, C. D., Massoli, P., Onasch, T. B., Forestieri, S. D., Martin, A. T., Cummings, M. J., Croasdale, D. R., Brune, W. H., Worsnop, D. R. and Davidovits, P.: Relationship between oxidation level and optical properties of secondary organic aerosol, Environ. Sci. Technol., 47, 6349–6357, doi:10.1021/es401043j, 2013.

Langridge, J. M., Richardson, M. S., Lack, D. A., Brock, C. A. and Murphy, D. M.: Limitations of the photoacoustic technique for aerosol absorption measurement at high relative humidity, Aerosol Sci. Technol., 47, 1163-1173, doi:10.1080/02786826.2013.827324, 2013.

Laskin, A., Laskin, J. and Nizkorodov, S. A.: Chemistry of atmospheric brown carbon, Chem. Rev., 115, 4335–4382, doi:10.1021/cr5006167, 2015.

Lee, A. K. Y., Zhao, R., Li, R., Liggio, J., Li, S.-M. and Abbatt, J. P. D.: Formation of light absorbing organo-nitrogen species from evaporation of droplets containing glyoxal and ammonium sulfate, Environ. Sci. Technol., 47, 12819–12826, doi:10.1021/es402687w, 2013.

Lee, H. J., Aiona, P. K., Laskin, A., Laskin, J. and Nizkorodov, S. A.: Effect of solar radiation on the optical properties and molecular composition of laboratory proxies of atmospheric brown carbon, Environ. Sci. Technol., 48, 10217–10226, doi:10.1021/es502515r, 2014.

Lee, L. and Wilson, K.: The reactive–diffusive length of OH and ozone in model organic aerosols, J. Phys. Chem. A, 120, 6800–6812, doi:10.1021/acs.jpca.6b05285, 2016.

Lewis, K., Arnott, W. P., Moosmüller, H. and Wold, C. E.: Strong spectral variation of biomass smoke light absorption and single scattering albedo observed with a novel dual-wavelength photoacoustic instrument, J. Geophys. Res. Atmospheres, 113, D16203, doi:10.1029/2007JD009699, 2008.

Li, Y. J., Huang, D. D., Cheung, H. Y., Lee, A. K. Y. and Chan, C. K.: Aqueous-phase photochemical oxidation and direct photolysis of vanillin – A model compound of methoxy phenols from biomass burning, Atmos. Chem. Phys., 14, 2871–2885, doi:10.5194/acp-14-2871-2014, 2014.

Lin, P., Aiona, P. K., Li, Y., Shiraiwa, M., Laskin, J., Nizkorodov, S. A. and Laskin, A.: Molecular characterization of brown carbon in biomass burning aerosol particles, Environ. Sci. Technol., 50, 11815–11824, doi:10.1021/acs.est.6b03024, 2016.

Lin, P., Bluvshtein, N., Rudich, Y., Nizkorodov, S. A., Laskin, J. and Laskin, A.: Molecular chemistry of atmospheric brown carbon inferred from a nationwide biomass burning event, Environ. Sci. Technol., 51, 11561-11570, doi:10.1021/acs.est.7b02276, 2017.

Liu, J., Bergin, M., Guo, H., King, L., Kotra, N., Edgerton, E. and Weber, R. J.: Size-resolved measurements of brown carbon in water and methanol extracts and estimates of their contribution to ambient fine-particle light absorption, Atmos. Chem. Phys., 13, 12389–12404, doi:10.5194/acp-13-12389-2013, 2013.

Nakayama, T., Sato, K., Matsumi, Y., Imamura, T., Yamazaki, A. and Uchiyama, A.: Wavelength and NO_x dependent complex refractive index of SOAs generated from the photooxidation of toluene, Atmos. Chem. Phys., 13, 531–545, doi:10.5194/acp-13-531-2013, 2013.

Ofner, J., Krüger, H.-U., Grothe, H., Schmitt-Kopplin, P., Whitmore, K. and Zetzsch, C.: Physico-chemical characterization of SOA derived from catechol and guaiacol – A model substance for the aromatic fraction of atmospheric HULIS, Atmos. Chem. Phys., 11, 1–15, doi:10.5194/acp-11-1-2011, 2011.

Pfrang, C., Shiraiwa, M. and Pöschl, U.: Coupling aerosol surface and bulk chemistry with a kinetic double layer model (K2-SUB): Oxidation of oleic acid by ozone, Atmos. Chem. Phys., 10, 4537–4557, doi:10.5194/acp-10-4537-2010, 2010.

Phillips, S. M. and Smith, G. D.: Light absorption by charge transfer complexes in brown carbon aerosols, Environ. Sci. Technol. Lett., 1, 382–386, doi:10.1021/ez500263j, 2014.

Phillips, S. M. and Smith, G. D.: Further evidence for charge transfer complexes in brown carbon aerosols from excitation–emission matrix fluorescence spectroscopy, J. Phys. Chem. A, 119, 4545–4551, doi:10.1021/jp510709e, 2015.

Pillar, E. A. and Guzman, M. I.: Oxidation of substituted catechols at the air–water interface: Production of carboxylic acids, quinones, and polyphenols, Environ. Sci. Technol., 51, 4951–4959, doi:10.1021/acs.est.7b00232, 2017.

Pillar, E. A., Camm, R. C. and Guzman, M. I.: Catechol oxidation by ozone and hydroxyl radicals at the air–water interface, Environ. Sci. Technol., 48, 14352–14360, doi:10.1021/es504094x, 2014.

Pillar, E. A., Zhou, R. and Guzman, M. I.: Heterogeneous oxidation of catechol, J. Phys. Chem. A, 119, 10349–10359, doi:10.1021/acs.jpca.5b07914, 2015.

Pöschl, U., Rudich, Y. and Ammann, M.: Kinetic model framework for aerosol and cloud surface chemistry and gas-particle interactions – Part 1: General equations, parameters, and terminology, Atmos. Chem. Phys., 7, 5989–6023, doi:10.5194/acp-7-5989-2007, 2007.

Radney, J. G., You, R., Zachariah, M. R. and Zangmeister, C. D.: Direct in situ mass specific absorption spectra of biomass burning particles generated from smoldering hard and softwoods, Environ. Sci. Technol., 51, 5622–5629, doi:10.1021/acs.est.7b00810, 2017.

Ramanathan, V. and Carmichael, G.: Global and regional climate changes due to black carbon, Nat. Geosci., 1, 221–227, doi:10.1038/ngeo156, 2008.

Raspet, R., Slaton, W. V., Arnott, W. P. and Moosmüller, H.: Evaporation–condensation effects on resonant photoacoustics of volatile aerosols, J. Atmospheric Ocean. Technol., 20, 685–695, doi:10.1175/1520-0426(2003)20<685:ECEORP>2.0.CO;2, 2003.

Richards-Henderson, N. K., Goldstein, A. H. and Wilson, K. R.: Large enhancement in the heterogeneous oxidation rate of organic aerosols by hydroxyl radicals in the presence of nitric oxide, J. Phys. Chem. Lett., 6, 4451–4455, doi:10.1021/acs.jpclett.5b02121, 2015.

Richards-Henderson, N. K., Goldstein, A. H. and Wilson, K. R.: Sulfur dioxide accelerates the heterogeneous oxidation rate of organic aerosol by hydroxyl radicals, Environ. Sci. Technol., 50, 3554–3561, doi:10.1021/acs.est.5b05369, 2016.

Rincón, A. G., Guzmán, M. I., Hoffmann, M. R. and Colussi, A. J.: Optical absorptivity versus molecular composition of model organic aerosol matter, J. Phys. Chem. A, 113, 10512–10520, doi:10.1021/jp904644n, 2009.

Saleh, R., Hennigan, C. J., McMeeking, G. R., Chuang, W. K., Robinson, E. S., Coe, H., Donahue, N. M. and Robinson, A. L.: Absorptivity of brown carbon in fresh and photo-chemically aged biomass-burning emissions, Atmos. Chem. Phys., 13, 7683–7693, doi:10.5194/acp-13-7683-2013, 2013.

Sareen, N., Moussa, S. G. and McNeill, V. F.: Photochemical aging of light-absorbing secondary organic aerosol material, J. Phys. Chem. A, 117, 2987–2996, doi:10.1021/jp309413j, 2013.

Schauer, J. J., Kleeman, M. J., Cass, G. R. and Simoneit, B. R. T.: Measurement of emissions from air pollution sources. 3. C_1–C_{29} organic compounds from fireplace combustion of wood, Environ. Sci. Technol., 35, 1716–1728, doi:10.1021/es001331e, 2001.

Shamjad, P. M., Tripathi, S. N., Thamban, N. M. and Vreeland, H.: Refractive index and absorption attribution of highly absorbing brown carbon aerosols from an urban Indian city-Kanpur, Sci. Rep., 6, 37735, doi:10.1038/srep37735, 2016.

Sharma, N., Arnold, I. J., Moosmüller, H., Arnott, W. P. and Mazzoleni, C.: Photoacoustic and nephelometric spectroscopy of aerosol optical properties with a supercontinuum light source, Atmos. Meas. Tech., 6, 3501–3513, doi:10.5194/amt-6-3501-2013, 2013.

Shiraiwa, M., Garland, R. M. and Pöschl, U.: Kinetic double-layer model of aerosol surface chemistry and gas-particle interactions (K2-SURF): Degradation of polycyclic aromatic hydrocarbons exposed to O3, NO2, H2O, OH and NO3, Atmos. Chem. Phys., 9, 9571–9586, doi:10.5194/acp-9-9571-2009, 2009.

Shiraiwa, M., Pfrang, C. and Pöschl, U.: Kinetic multi-layer model of aerosol surface and bulk chemistry (KM-SUB): The influence of interfacial transport and bulk diffusion on the oxidation of oleic acid by ozone, Atmos. Chem. Phys., 10, 3673–3691, doi:10.5194/acp-10-3673-2010, 2010.

Simoneit, B. R. T.: Biomass burning — A review of organic tracers for smoke from incomplete combustion, Appl. Geochem., 17, 129–162, doi:10.1016/S0883-2927(01)00061-0, 2002.

Smith, J. D., Kinney, H. and Anastasio, C.: Phenolic carbonyls undergo rapid aqueous photodegradation to form low-volatility, light-absorbing products, Atmos. Environ., 126, 36–44, doi:10.1016/j.atmosenv.2015.11.035, 2016.

Song, M., Liu, P. F., Hanna, S. J., Li, Y. J., Martin, S. T. and Bertram, A. K.: Relative humidity-dependent viscosities of isoprene-derived secondary organic material and atmospheric implications for isoprene-dominant forests, Atmos. Chem. Phys., 15, 5145–5159, doi:10.5194/acp-15-5145-2015, 2015.

Song, M., Liu, P. F., Hanna, S. J., Zaveri, R. A., Potter, K., You, Y., Martin, S. T. and Bertram, A. K.: Relative humidity-dependent viscosity of secondary organic material from toluene photo-oxidation and possible implications for organic particulate matter over megacities, Atmos. Chem. Phys., 16, 8817–8830, doi:10.5194/acp-16-8817-2016, 2016.

von Sonntag, C. and Schuchmann, H.-P.: The elucidation of peroxyl radical reactions in aqueous solution with the help of radiation-chemical methods, Angew. Chem. Int. Ed. Engl., 30, 1229–1253, doi:10.1002/anie.199112291, 1991.

Sumlin, B. J., Pandey, A., Walker, M. J., Pattison, R. S., Williams, B. J. and Chakrabarty, R. K.: Atmospheric photooxidation diminishes light absorption by primary brown carbon aerosol from biomass burning, Environ. Sci. Technol. Lett., 4, 540-545, doi:10.1021/acs.estlett.7b00393, 2017.

Sun, H., Biedermann, L. and Bond, T. C.: Color of brown carbon: A model for ultraviolet and visible light absorption by organic carbon aerosol, Geophys. Res. Lett., 34, L17813, doi:10.1029/2007GL029797, 2007.

Sun, Y. L., Zhang, Q., Anastasio, C. and Sun, J.: Insights into secondary organic aerosol formed via aqueous-phase reactions of phenolic compounds based on high resolution mass spectrometry, Atmos. Chem. Phys., 10, 4809–4822, doi:10.5194/acp-10-4809-2010, 2010.

Tang, M., Alexander, J. M., Kwon, D., Estillore, A. D., Laskina, O., Young, M. A., Kleiber, P. D. and Grassian, V. H.: Optical and physicochemical properties of brown carbon aerosol: Light scattering, FTIR extinction spectroscopy, and hygroscopic growth, J. Phys. Chem. A, 120, 4155–4166, doi:10.1021/acs.jpca.6b03425, 2016.

Tasoglou, A., Saliba, G., Subramanian, R. and Pandis, S. N.: Absorption of chemically aged biomass burning carbonaceous aerosol, J. Aerosol Sci., 113(Supplement C), 141–152, doi:10.1016/j.jaerosci.2017.07.011, 2017.

Teich, M., van Pinxteren, D., Wang, M., Kecorius, S., Wang, Z., Müller, T., Močnik, G. and Herrmann, H.: Contributions of nitrated aromatic compounds to the light absorption of water-soluble and particulate brown carbon in different atmospheric environments in Germany and China, Atmos. Chem. Phys., 17, 1653–1672, doi:10.5194/acp-17-1653-2017, 2017.

Tóth, A., Hoffer, A., Nyirő-Kósa, I., Pósfai, M. and Gelencsér, A.: Atmospheric tar balls: Aged primary droplets from biomass burning?, Atmos. Chem. Phys., 14, 6669–6675, doi:10.5194/acp-14-6669-2014, 2014.

Veres, P., Roberts, J. M., Burling, I. R., Warneke, C., de Gouw, J. and Yokelson, R. J.: Measurements of gas-phase inorganic and organic acids from biomass fires by negative-ion proton-transfer chemical-ionization mass spectrometry, J. Geophys. Res. Atmos. 115, D23302, doi:10.1029/2010JD014033, 2010.

Virkkula, A., Koponen, I. K., Teinilä, K., Hillamo, R., Kerminen, V.-M. and Kulmala, M.: Effective real refractive index of dry aerosols in the Antarctic boundary layer, Geophys. Res. Lett., 33, L06805, doi:10.1029/2005GL024602, 2006.

Wang, Z., Bi, X., Sheng, G. and Fu, J.: Characterization of organic compounds and molecular tracers from biomass burning smoke in South China I: Broad-leaf trees and shrubs, Atmos. Environ., 43, 3096–3102, doi:10.1016/j.atmosenv.2009.03.012, 2009.

Wiegand, J. R., Mathews, L. D. and Smith, G. D.: A UV–Vis photoacoustic spectrophotometer, Anal. Chem., 86, 6049–6056, doi:10.1021/ac501196u, 2014.

Wiegel, A. A., Liu, M. J., Hinsberg, W. D., Wilson, K. R. and Houle, F. A.: Diffusive confinement of free radical intermediates in the OH radical oxidation of semisolid aerosols, Phys. Chem. Chem. Phys., 19, 6814–6830, doi:10.1039/C7CP00696A, 2017.

Wong, J. P. S., Zhou, S. and Abbatt, J. P. D.: Changes in secondary organic aerosol composition and mass due to photolysis: Relative humidity dependence, J. Phys. Chem. A, 119, 4309–4316, doi:10.1021/jp506898c, 2015.

Wong, J. P. S., Nenes, A. and Weber, R. J.: Changes in light absorptivity of molecular weight separated brown carbon due to photolytic aging, Environ. Sci. Technol., 51, 8414-8421, doi:10.1021/acs.est.7b01739, 2017.

Yu, G., Bayer, A. R., Galloway, M. M., Korshavn, K. J., Fry, C. G. and Keutsch, F. N.: Glyoxal in aqueous ammonium sulfate solutions: Products, kinetics and hydration effects, Environ. Sci. Technol., 45, 6336–6342, doi:10.1021/es200989n, 2011.

Yu, L., Smith, J., Laskin, A., Anastasio, C., Laskin, J. and Zhang, Q.: Chemical characterization of SOA formed from aqueous-phase reactions of phenols with the triplet excited state of carbonyl and hydroxyl radical, Atmos. Chem. Phys., 14, 13801–13816, doi:10.5194/acp-14-13801-2014, 2014.

Yu, L., Smith, J., Laskin, A., George, K. M., Anastasio, C., Laskin, J., Dillner, A. M. and Zhang, Q.: Molecular transformations of phenolic SOA during photochemical aging in the aqueous phase: Competition among oligomerization, functionalization, and fragmentation, Atmos. Chem. Phys., 16, 4511–4527, doi:10.5194/acp-16-4511-2016, 2016.

Zhang, L., Peslherbe, G. H. and Muchall, H. M.: A general measure of conjugation in biphenyls and their radical cations, Can. J. Chem., 88, 1175–1185, doi:10.1139/V10-126, 2010.

Zhang, X., Huang, Y., Rao, R. and Wang, Z.: Retrieval of effective complex refractive index from intensive measurements of characteristics of ambient aerosols in the boundary layer, Opt. Express, 21, 17849–17862, 2013.

Zhang, Y., Forrister, H., Liu, J., Dibb, J., Anderson, B., Schwarz, J. P., Perring, A. E., Jimenez, J. L., Campuzano-Jost, P., Wang, Y., Nenes, A. and Weber, R. J.: Top-of-atmosphere radiative forcing affected by brown carbon in the upper troposphere, Nat. Geosci., 10, 486–489, doi:10.1038/ngeo2960, 2017.

Zhao, R., Lee, A. K. Y., Huang, L., Li, X., Yang, F. and Abbatt, J. P. D.: Photochemical processing of aqueous atmospheric brown carbon, Atmos. Chem. Phys., 15, 6087–6100, doi:10.5194/acp-15-6087-2015, 2015.

Zhong, M. and Jang, M.: Dynamic light absorption of biomass-burning organic carbon photochemically aged under natural sunlight, Atmos. Chem. Phys., 14, 1517–1525, doi:10.5194/acp-14-1517-2014, 2014.

Ziemann, P. J.: Aerosol products, mechanisms, and kinetics of heterogeneous reactions of ozone with oleic acid in pure and mixed particles, Faraday Discuss., 130, 469–490, doi:10.1039/B417502F, 2005.

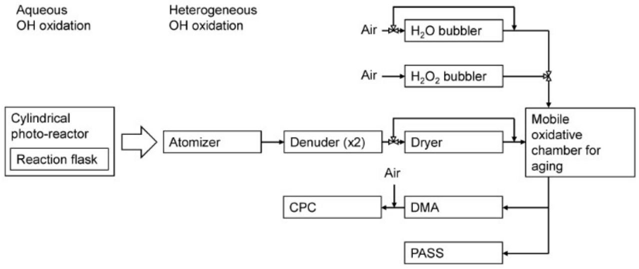

Figure 1. Experimental setup during aqueous and heterogeneous OH oxidation. CPC: condensational particle counter; DMA: differential mobility analyzer; PASS: photo-acoustic spectrometer.

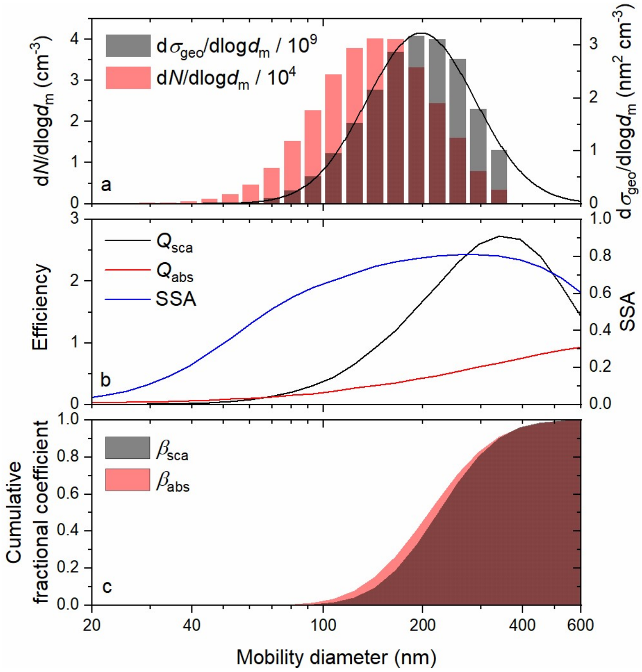

Figure 2. Representative (a) number- and geometric-cross-section-weighted size distributions, (b) predicted scattering and absorption efficiencies and SSA, based on an assumed complex refractive index of $m = 1.35 + 0.41i$, and (c) cumulative fractional scattering and absorption coefficients, based on the observed size distribution and predicted efficiencies.

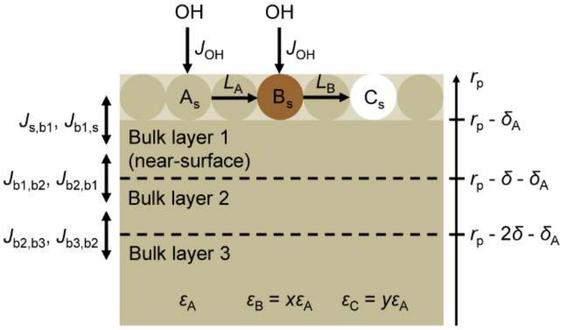

Figure 3. Schematic of the multi-layer kinetics model of heterogeneous OH oxidation.

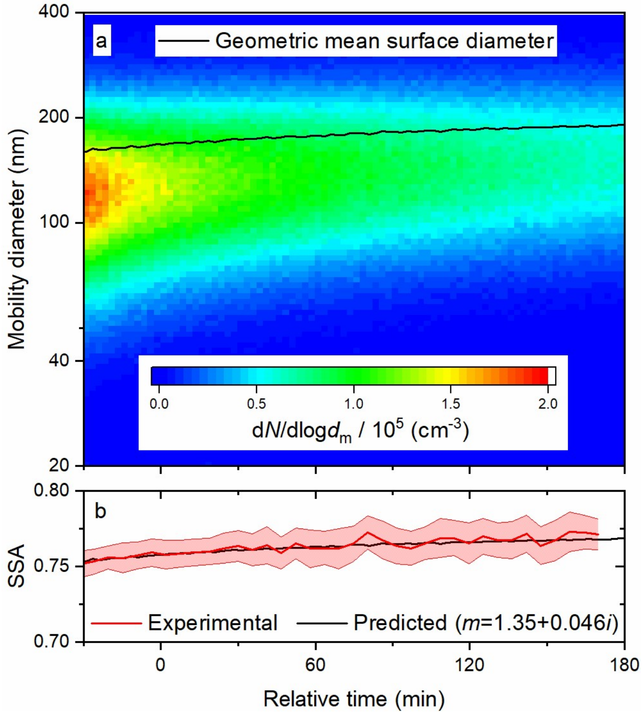

Figure 4. Time series of (a) size distribution and geometric surface diameter and (b) predicted (based on size distributions) and observed SSA during a deposition experiment at 60% RH. In (b), the upper and lower bounds illustrate one standard deviation about the 5-minute averages.

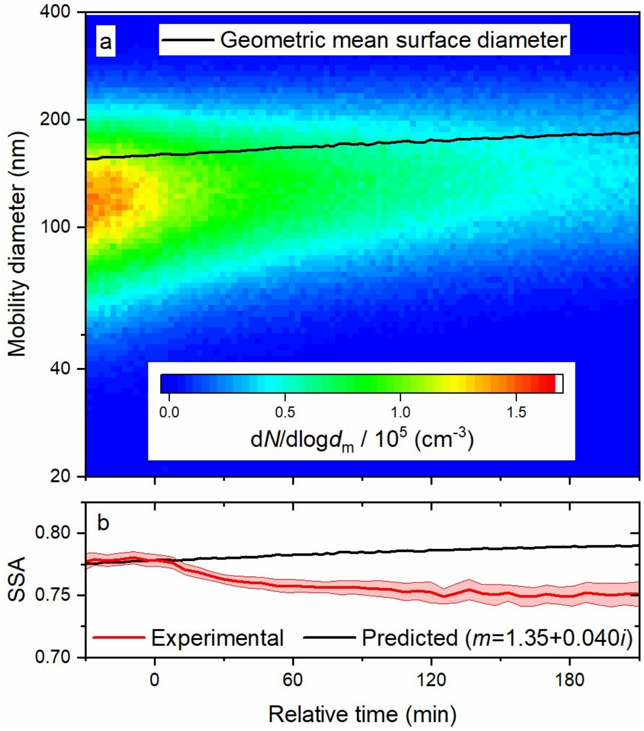

Figure 5. Time series of (a) size distribution and geometric surface diameter and (b) predicted (based on size distributions) and observed SSA during a photolysis experiment at 60% RH. In (b), the upper and lower bounds illustrate one standard deviation about the 5-minute averages.

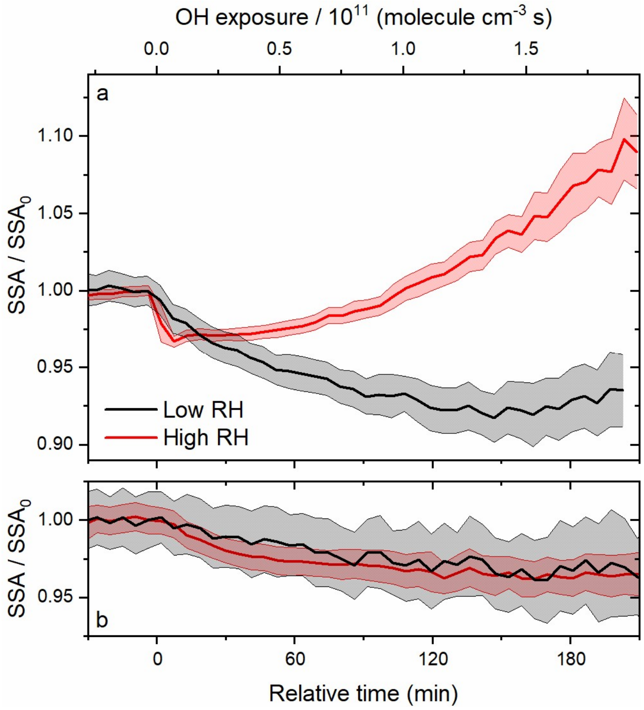

Figure 6. Time series of relative SSA during (a) heterogeneous OH oxidation and (b) photolysis experiments at 15 and 60% RH.

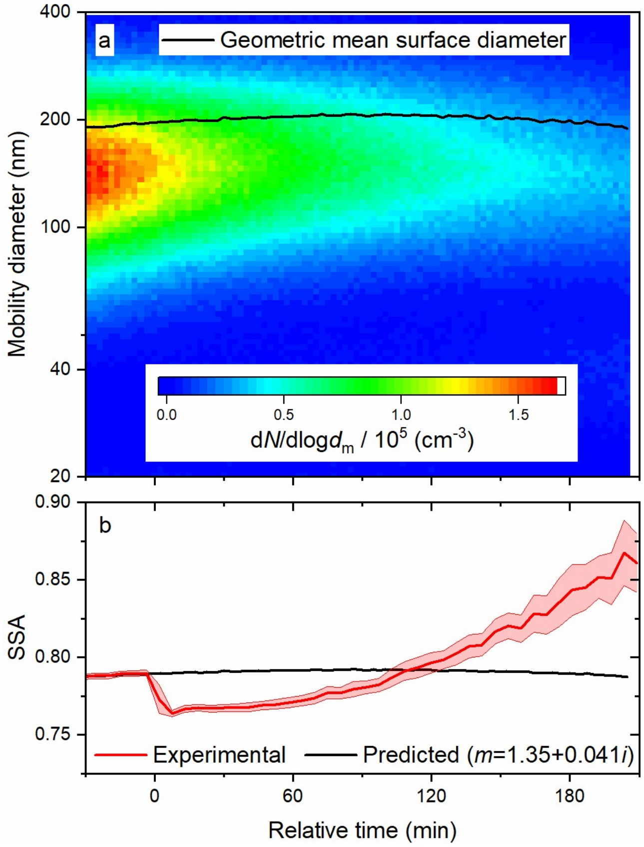

Figure 7. Time series of (a) size distribution and geometric surface diameter and (b) predicted (based on size distributions) and observed SSA during a photo-oxidation experiment at 60% RH. In (b), the upper and lower bounds illustrate one standard deviation about the 5-minute averages.

5

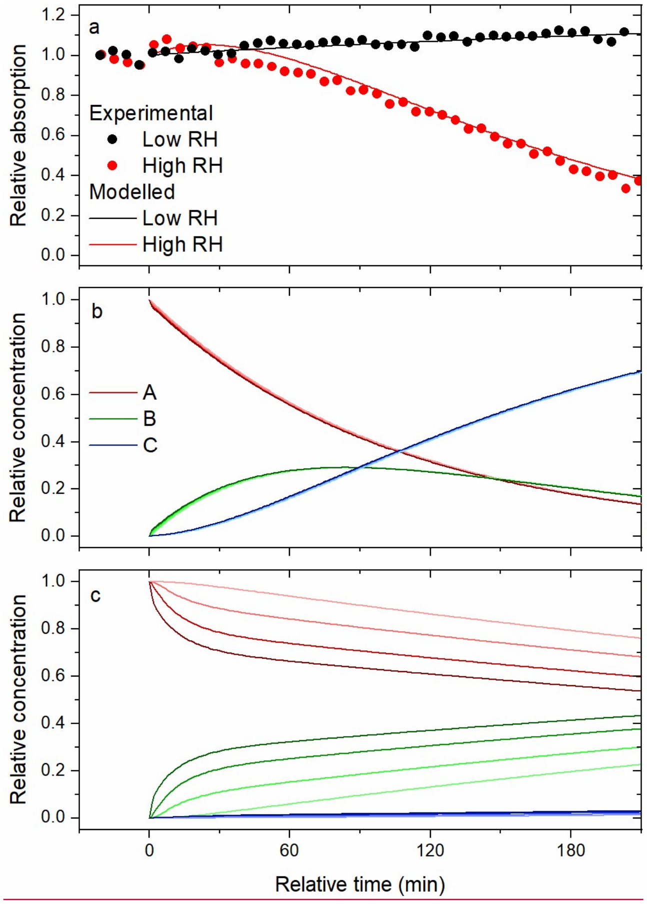

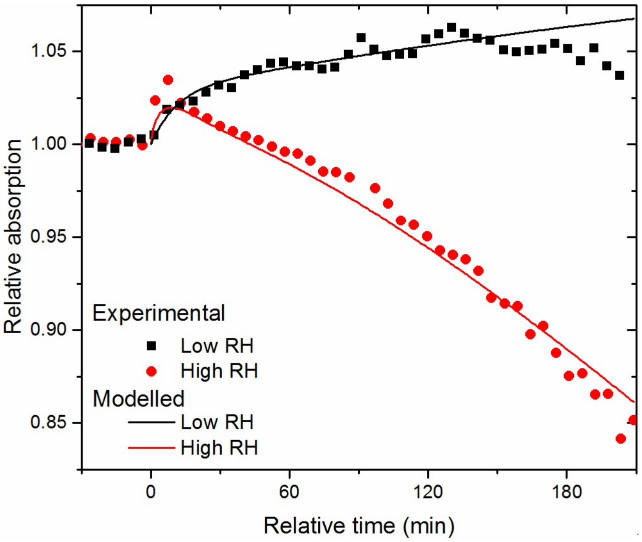

Figure 8. Time series of (a) observed and modelled relative absorption at 60 and 15% RH and the modelled relative concentrations of A, B, and C at (b) 60% RH and (c) 15% RH. The curves are shaded according to layer, with the darkest curves corresponding to the surface layer.~~Time series of observed and modelled relative absorption at 15 and 60% RH. The experimental trends are the inverse of relative SSA.~~

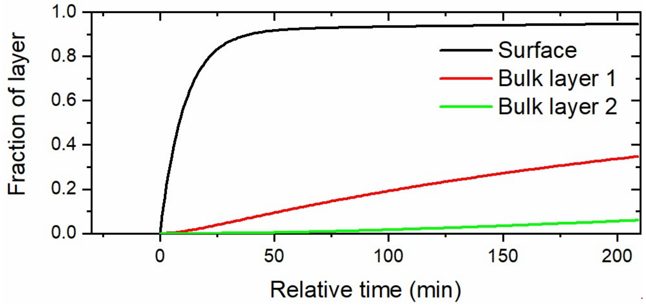

~~**Figure 9.** Modelled fraction of surface and bulk layers 1 and 2 composed of products B and C at 15% RH.~~

Supporting Information for “Heterogeneous OH oxidation of secondary brown carbon aerosol”

Elijah G. Schnitzler, Jonathan P. D. Abbatt

Department of Chemistry, University of Toronto, Toronto, ON, M5S 3H6, Canada

Correspondence to: Jonathan P. D. Abbatt (jabbatt@chem.utoronto.ca)

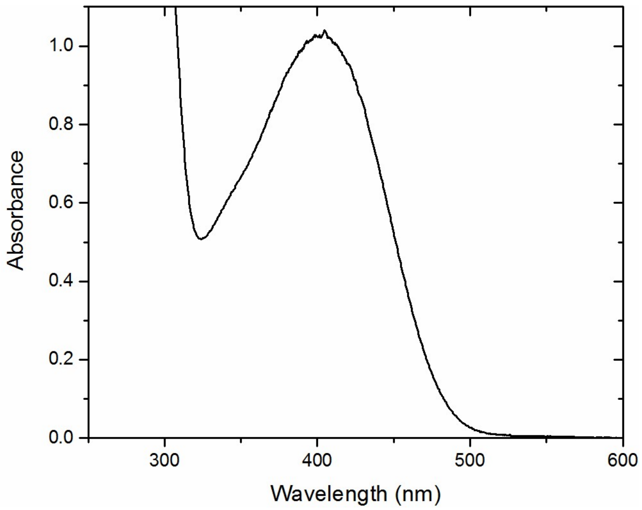

Figure S1. Absorption spectrum of Cibacron Brilliant Yellow 3G-P dye solution.

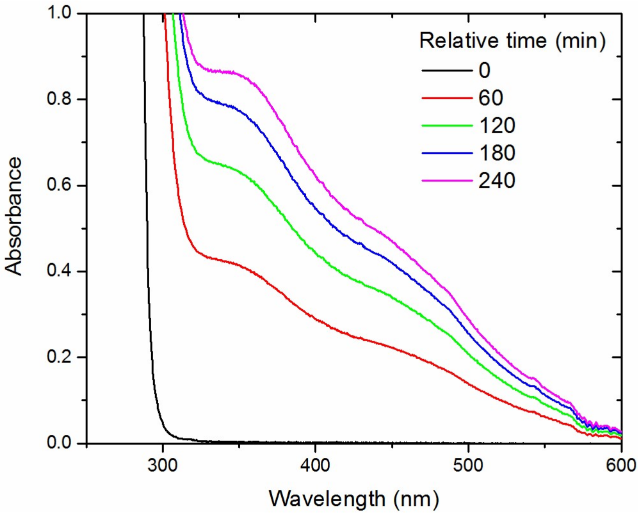

Figure S2. Absorption spectra of the resorcinol product mixture at different irradiation times.

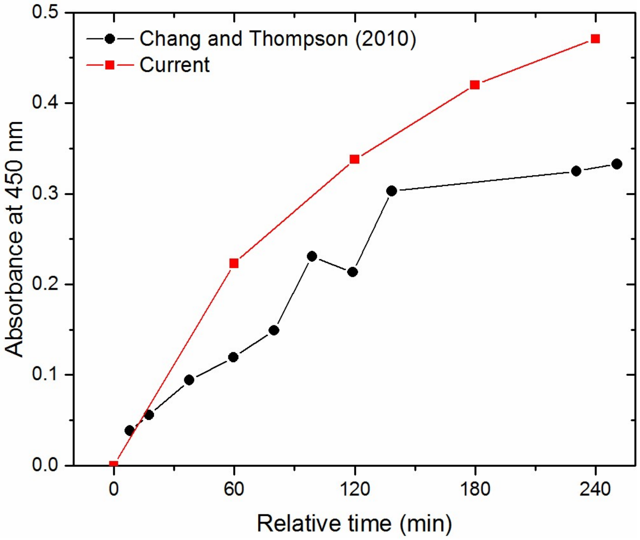

Figure S3. Absorbance at 450 nm of resorcinol product mixture as a function of irradiation time.

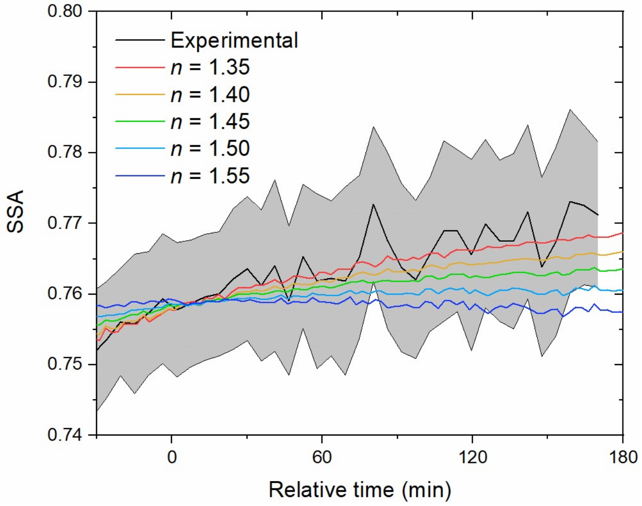

Figure S4. Time series of observed and predicted (based on the size distributions) SSA during a deposition experiment.

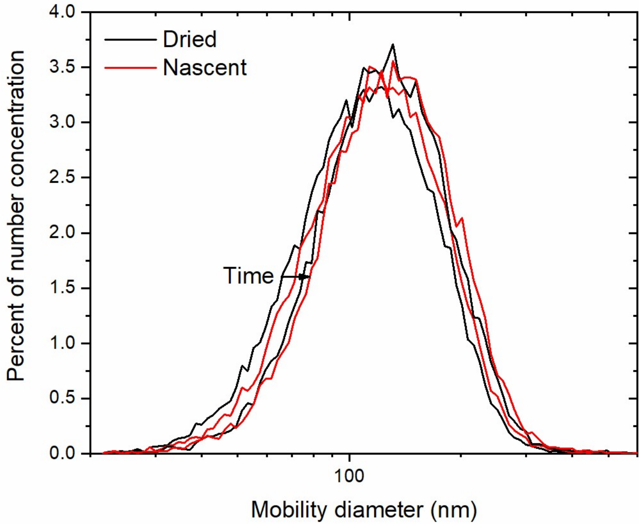

Figure S5. Size distributions of dried and nascent particles, collected alternately in 15 min intervals.

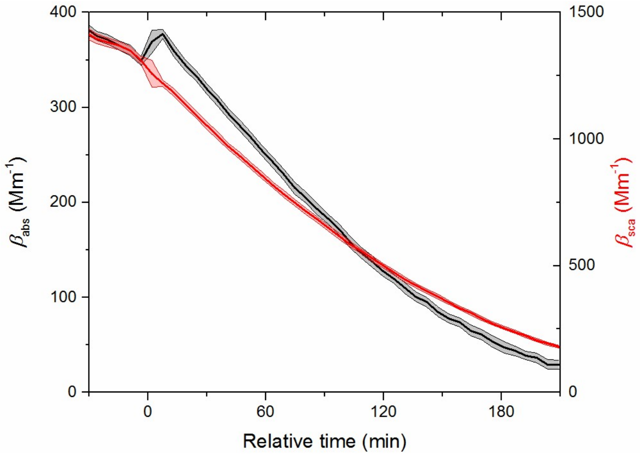

Figure ~~S4~~S6. Time series of absorption and scattering coefficients of the secondary BrC surrogate during a heterogeneous OH oxidation experiment at high RH.

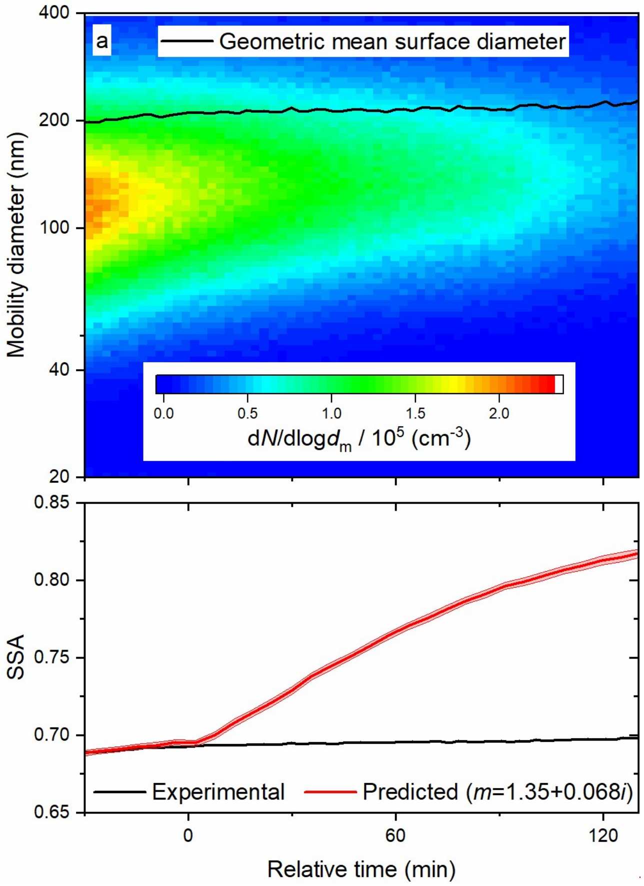

~~**Figure S5.** Time series of (a) size distribution and geometric mean surface diameter and (b) predicted (based on size distributions) and observed SSA of the yellow dye aerosol during heterogeneous OH oxidation at high RH. In (b), the upper and lower bounds illustrate one standard deviation about the 5-minute averages.~~

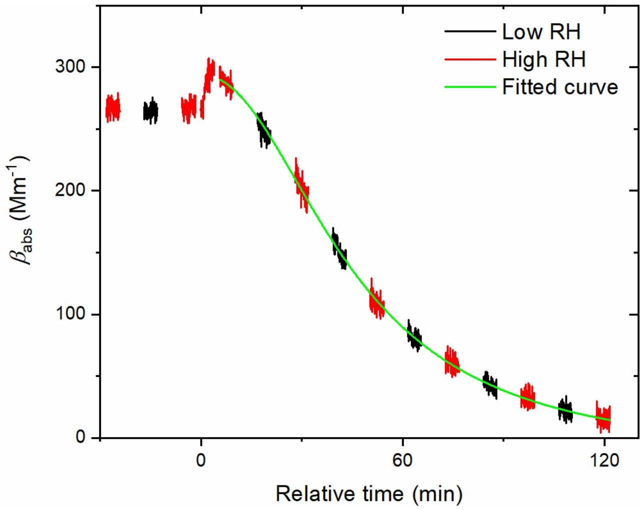

Figure S7. Time series of the absorption coefficient at 405 nm for dried and nascent particles.

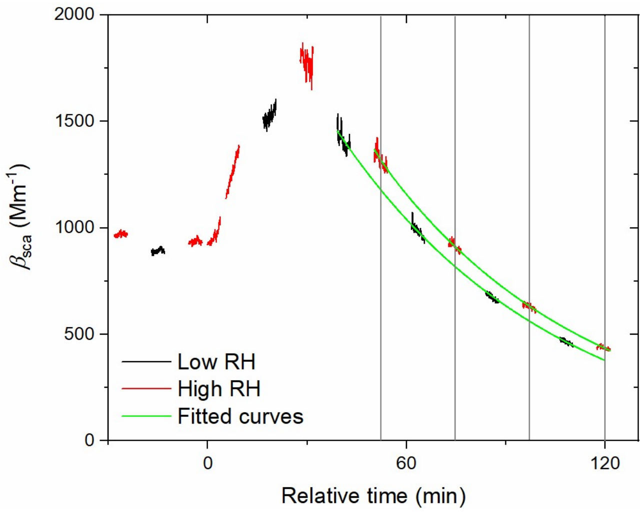

Figure S8. Time series of the scattering coefficient at 405 nm for dried and nascent particles. (The particle growth observed early in this experiment, leading to an increase in the scattering coefficient, did not occur for any other experiments.)

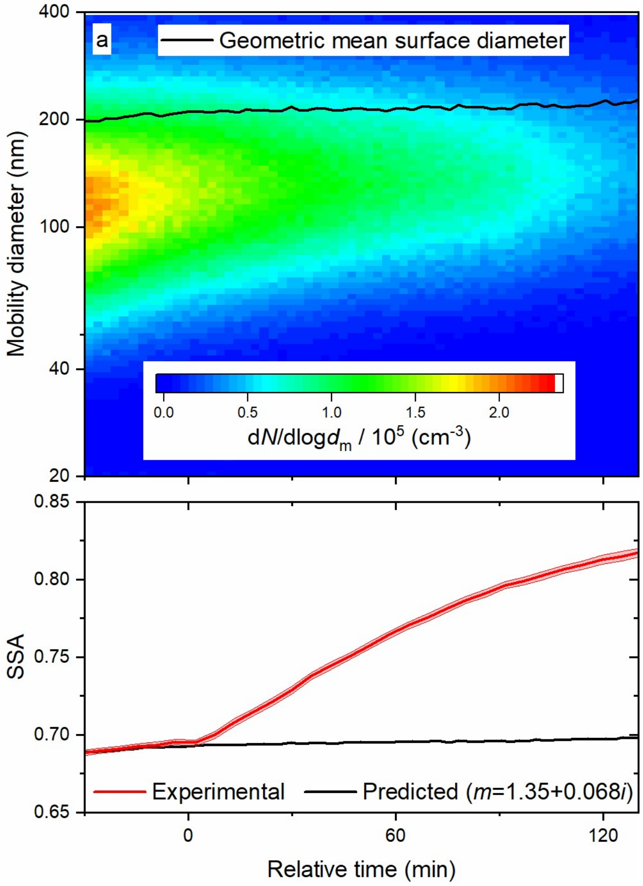

Figure S9. Time series of (a) size distribution and geometric mean surface diameter and (b) predicted (based on size distributions) and observed SSA of the yellow dye aerosol during heterogeneous OH oxidation at high RH. In (b), the upper and lower bounds illustrate one standard deviation about the 5-minute averages.

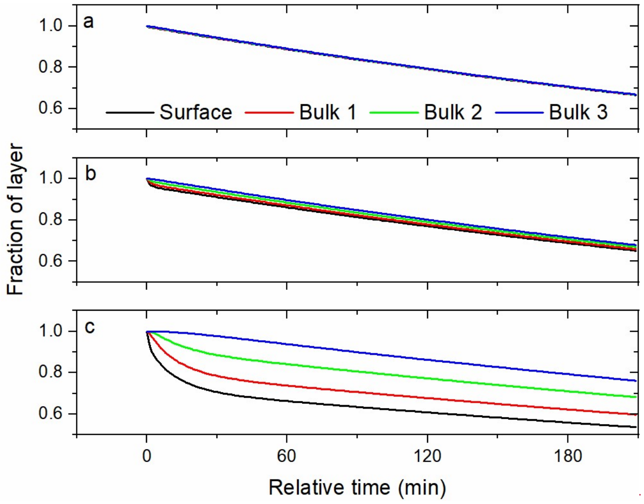

~~**Figure S6.** The fraction of each layer composed of species A when the diffusion coefficient is set to (a) 1 x 10^{-14} cm^2 s^{-1}, (b) 1 x 10^{-15} cm^2 s^{-1}, and (c) 1 x 10^{-16} cm^2 s^{-1}.~~

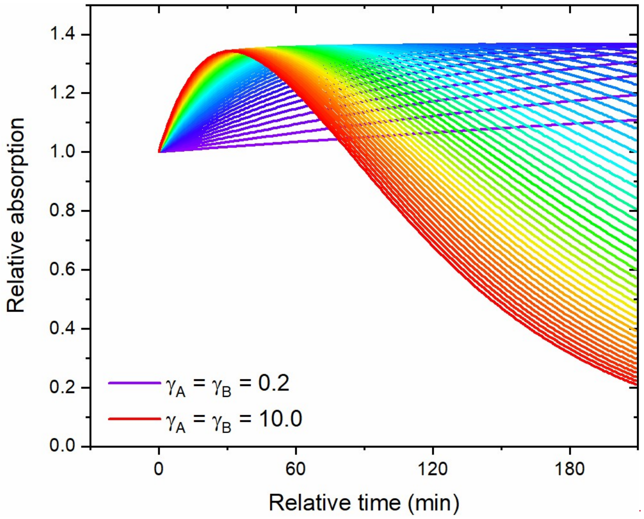

~~**Figure S7.** The relative absorption when the diffusion coefficient is set to 1 x 10^{-14} cm^2 s^{-1}, the absorptivities are fixed, and the uptake coefficient is scanned from 0.2 to 10.~~

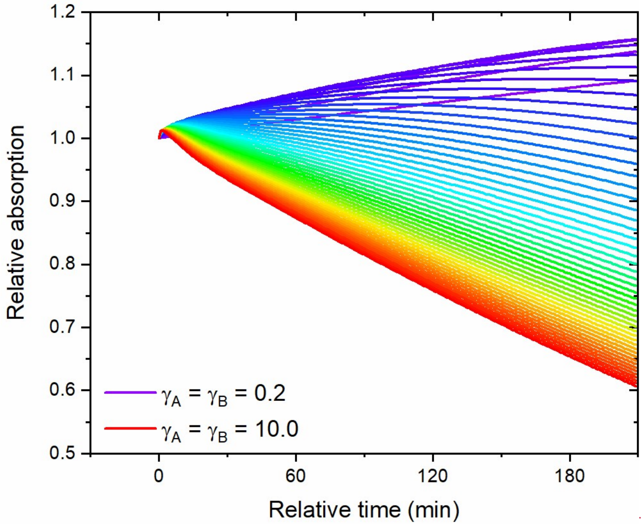

~~**Figure S8.** The relative absorption when the diffusion coefficient is set to 1 x 10^{-16} cm^2 s^{-1}, the absorptivities are fixed, and the uptake coefficient is scanned from 0.2 to 10.~~

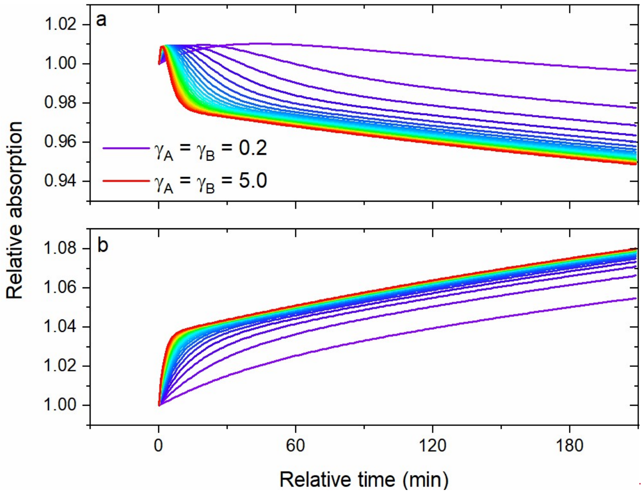

~~**Figure S9.** The relative absorption when the diffusion coefficient is set to 1 x 10^{-18} cm^2 s^{-1}, the absorptivities are fixed, and the uptake coefficient is scanned from 0.2 to 5. In (a), species B is absorbing, species C is colourless, and the absorption decays away. In (b), both species B and C are absorbing, and the absorption persists.~~